2020

Increased Ecological Resource Variability during a Critical Transition in Hominin Evolution

Richard Potts

René Dommain

Jessica W. Moerman

Anna K. Behrensmeyer

Alan L. Deino

See next page for additional authors

Citation/Publisher Attribution

Potts, R. et al. (2020) Increased ecological resource variability during a critical transition in hominin evolution. *Science Advances*. 6(43) eabc8975. DOI: 10.1126/sciadv.abc8975

EVOLUTIONARY BIOLOGY

Increased ecological resource variability during a critical transition in hominin evolution

Richard Potts[1,2]*, René Dommain[1,3], Jessica W. Moerman[1], Anna K. Behrensmeyer[4], Alan L. Deino[5], Simon Riedl[3], Emily J. Beverly[6], Erik T. Brown[7], Daniel Deocampo[8], Rahab Kinyanjui[2], Rachel Lupien[9], R. Bernhart Owen[10], Nathan Rabideaux[11], James M. Russell[12], Mona Stockhecke[7,13], Peter deMenocal[9], J. Tyler Faith[14,15], Yannick Garcin[16], Anders Noren[17], Jennifer J. Scott[18], David Western[19], Jordon Bright[20], Jennifer B. Clark[1], Andrew S. Cohen[21], C. Brehnin Keller[22], John King[23], Naomi E. Levin[24], Kristina Brady Shannon[17], Veronica Muiruri[2], Robin W. Renaut[25], Stephen M. Rucina[2], Kevin Uno[9]

Although climate change is considered to have been a large-scale driver of African human evolution, landscape-scale shifts in ecological resources that may have shaped novel hominin adaptations are rarely investigated. We use well-dated, high-resolution, drill-core datasets to understand ecological dynamics associated with a major adaptive transition in the archeological record ~24 km from the coring site. Outcrops preserve evidence of the replacement of Acheulean by Middle Stone Age (MSA) technological, cognitive, and social innovations between 500 and 300 thousand years (ka) ago, contemporaneous with large-scale taxonomic and adaptive turnover in mammal herbivores. Beginning ~400 ka ago, tectonic, hydrological, and ecological changes combined to disrupt a relatively stable resource base, prompting fluctuations of increasing magnitude in freshwater availability, grassland communities, and woody plant cover. Interaction of these factors offers a resource-oriented hypothesis for the evolutionary success of MSA adaptations, which likely contributed to the ecological flexibility typical of *Homo sapiens* foragers.

INTRODUCTION

Hypotheses linking environmental change with human evolution have focused on temporal correlations between global or regional climate change and major evolutionary benchmarks. For African hominin evolution, one approach is to identify how increased aridity, humidity, or climate variability induced by orbital forcing broadly coincided with, and thus potentially initiated, the emergence of hominin adaptations and speciation events over time (*1*–*5*). It is not yet clear, however, whether any of these general paleoclimate hypotheses account for critical transitions in hominin evolution. A continuing challenge is to connect climate and environmental records with water availability, food, and other ecological resources critical to energy acquisition, yet susceptible to changes that may undermine an organism's existing adaptive strategies. Here, we integrate high-resolution drill core data with outcrop records from adjacent sub-basins in the southern Kenyan Rift Valley to examine how shifts in landscape-scale ecological resources could have influenced hominin adaptation during an interval of fundamental archeological and paleontological change in this region.

The sedimentary record recovered by the Olorgesailie Drilling Project (core ODP-OLO12-1A) from the Koora basin (1.8°S, 36.4°E) provides evidence for changes in water availability, vegetation, and overall resource landscapes associated with the demise of the Acheulean—the longest enduring Paleolithic technology—and its replacement by early Middle Stone Age (MSA) technology as documented in the adjacent Olorgesailie basin (1.5° to 1.6°S, 36.4° to 36.5°E; Fig. 1). Olorgesailie preserves the oldest evidence currently known in East Africa of the permanent loss of the Acheulean (defined by handaxes and other large cutting tools) and the emergence of MSA behavioral innovations (*6*, *7*). This transition involved new technologies, long-distance obsidian transfer indicating resource exchange among interconnected social groups, and the use of coloring material potentially related to enhanced symbolic capability (Table 1).

[1]Human Origins Program, National Museum of Natural History, Smithsonian Institution, Washington, DC 20013, USA. [2]Department of Earth Sciences, National Museums of Kenya, P.O. Box 40658, Nairobi 00100, Kenya. [3]Institute of Geosciences, University of Potsdam, 14476 Potsdam, Germany. [4]Department of Paleobiology, National Museum of Natural History, Smithsonian Institution, Washington, DC 20013, USA. [5]Berkeley Geochronology Center, Ridge Road, Berkeley, CA 94709, USA. [6]Earth and Atmospheric Sciences, University of Houston, TX 77204, USA. [7]Large Lakes Observatory and Dept. of Earth and Environmental Sciences, University of Minnesota Duluth, Duluth, MN 55812, USA. [8]Department of Geosciences, Georgia State University, Atlanta, GA 30302, USA. [9]Lamont-Doherty Earth Observatory, Columbia University, Palisades, NY 10964, USA. [10]Department of Geography, Hong Kong Baptist University, Kowloon Tong, Hong Kong. [11]Department of Chemistry, Rutgers University Newark, Newark, NJ 07109, USA. [12]Department of Earth, Environmental, and Planetary Sciences, Brown University, Providence, RI 02912, USA. [13]Department of Surface Waters-Research and Management, EAWAG, Überlandstr. 133, 8600 Dübendorf, Switzerland. [14]Natural History Museum of Utah, University of Utah, Salt Lake City, UT 84108, USA. [15]Department of Anthropology, University of Utah, Salt Lake City, UT 84112, USA. [16]Aix Marseille Univ, CNRS, IRD, INRAE, Coll France, CEREGE, 13545 Aix-en-Provence, France. [17]Continental Scientific Drilling Coordination Office and LacCore Facility, Dept. of Earth and Environmental Sciences, University of Minnesota, Minneapolis, MN 55455, USA. [18]Department of Earth and Environmental Sciences, Mount Royal University, Calgary, Alberta T3E 6K6, Canada. [19]African Conservation Centre, P.O. Box 15289, Nairobi 00509, Kenya. [20]School of Earth and Sustainability, Northern Arizona University, Flagstaff, AZ 86011, USA. [21]Department of Geosciences, University of Arizona, Tucson, AZ 85721, USA. [22]Department of Earth Sciences, Dartmouth College, Hanover, NH 03755, USA. [23]Graduate School of Oceanography, University of Rhode Island, Narragansett, RI 02882, USA. [24]Department of Earth and Environmental Sciences, University of Michigan, Ann Arbor, MI 48109, USA. [25]Department of Geological Sciences, University of Saskatchewan, Saskatoon, SK S7N 5E2, Canada.
*Corresponding author. Email: pottsr@si.edu

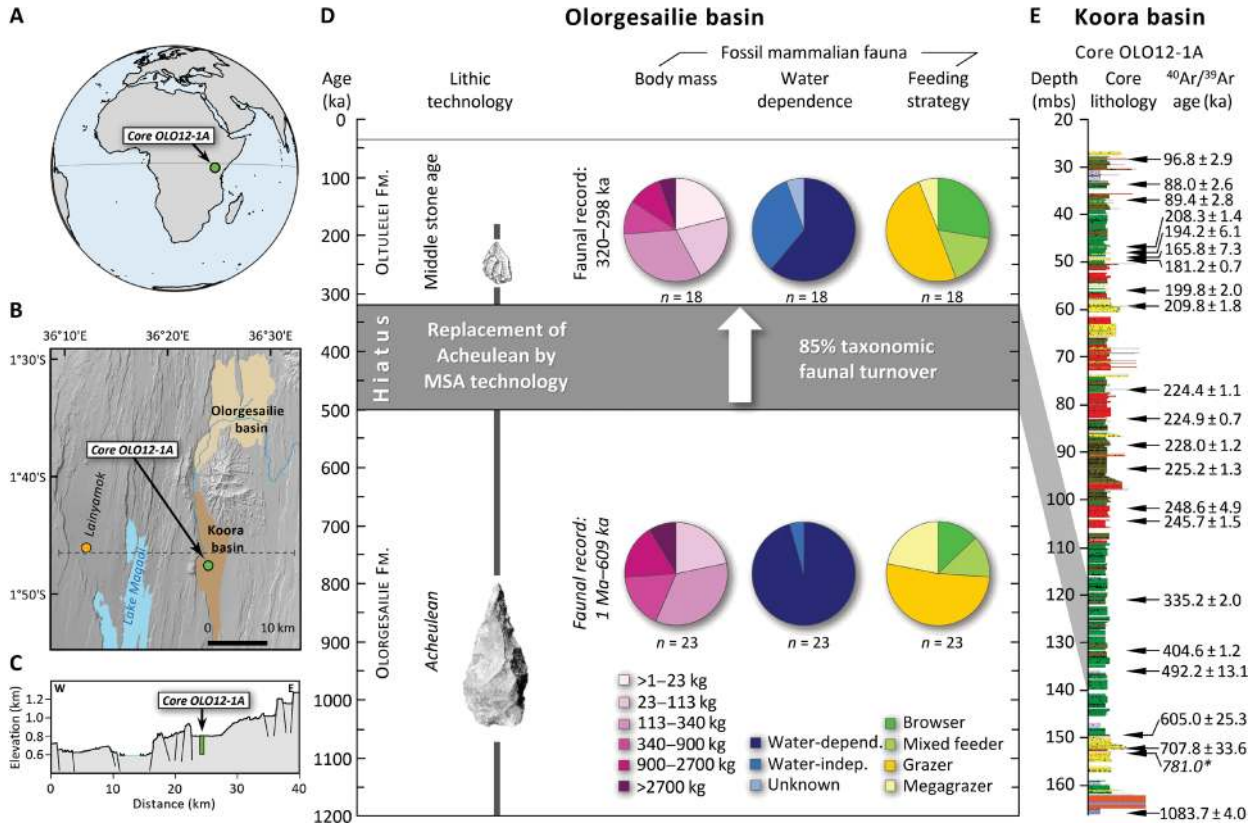

Fig. 1. Archeological and faunal transitions in the Olorgesailie basin and location, lithology, and geochronology of the Olorgesailie Drilling Project core OLO12-1A. (**A** to **C**) Locations of Koora basin drill core, Olorgesailie, Lainyamok fossil site, and east-to-west faulted topography (cross section). (**D**) Olorgesailie basin Acheulean technology spanning ~1 Ma to 500 ka ago; replacement by Middle Stone Age technology ~320 ka ago; and turnover in the fossil mammalian fauna (*6*–*8*), including community-level change in body mass, water dependence, and feeding strategies (table S1). Fossil assemblages dated between ~397 and 300 ka ago recording the faunal turnover are from Olorgesailie and Lainyamok (*7*, *8*, *43*). The hominin behavioral and faunal transitions in the Olorgesailie basin occurred during an erosional hiatus dated ~500 to 320 ka old. (Map image: TanDEM-X DEM DLR; tool images: Smithsonian Institution.) (**E**) Koora basin drill core depth (meters below surface), lithological sequence, and age constraints spanning from ~1.084 Ma to ~83.5 ka ago, based on Bayesian age model ($^{40}Ar/^{39}Ar$ ages ± 1σ and Brunhes/Matuyama magnetostratigraphic boundary*) (*19*). Shaded zone indicates drill core lithological record during the hiatus in the Olorgesailie outcrop record. See Fig. 2, fig. S1 (lithological key), and Materials and Methods.

The onset of these behavioral innovations in the southern Kenya rift occurred between 500 and 320 thousand years (ka) ago (Fig. 1) (*8*), an interval that overlaps the estimated time of genomic divergence between *Homo sapiens* in Africa and the Neanderthal-Denisovan clade in Eurasia (*9*). The oldest, widely acknowledged fossil evidence of *H. sapiens* (Jebel Irhoud, Morocco), dated roughly 320 to 300 ka old (*10*), coincided temporally with the oldest East African MSA evidence at Olorgesailie. Although other hominin species, such as *H. heidelbergensis* [or *H. rhodesiensis*, e.g., Kabwe, Zambia; (*11*)] and *Homo naledi* [Rising Star Cave, South Africa; (*12*)] were also present in Africa at this time, neither of these taxa is securely associated with MSA artifacts, whereas the MSA is widely associated from 300 ka ago onward with early *H. sapiens* (*13*, *14*). Hominin remains from southern Kenya dated 397 to 334 ka old consist of poorly preserved teeth and a femoral shaft from Lainyamok (Fig. 1A), which are metrically consistent with early *H. sapiens* but otherwise cannot distinguish archaic and modern humans (*15*, *16*). Other cranial remains of late middle Pleistocene age in eastern Africa typically combine *H. sapiens* and archaic traits, yet these finds are either poorly constrained chronologically (e.g., Eliye Springs KNM-ES 11693, Kenya) or <200 ka old (e.g., Guomde Formation KNM-ER 3884, Kenya; Eyasi 1 and 2, Ngaloba LH 18, Tanzania; Kibish Formation Omo 1 and 2, Herto BOU-VP-16/1, Ethiopia) [reviewed in (*17*)].

Our study does not presume that either the MSA or *H. sapiens* originated in the southern Kenya rift. This region, however, has yielded what is currently the oldest record with precise dating (*8*) where MSA behavioral innovations permanently replaced the Acheulean.

In the southern Kenya rift, the Acheulean-to-MSA archeological transition was accompanied by a massive, ~85% turnover in mammalian species between ~394 and 320 ka ago (*7*). As part of the turnover, previously dominant megaherbivores disappear from the record ("megagrazers": body mass > 900 kg), while smaller, water-independent, mixed grazing/browsing herbivores increased in abundance (Fig. 1D and table S1).

An important motivation of our study is that an erosional hiatus occurs in the Olorgesailie basin outcrop record between 500 and 320 ka ago—the interval in which the behavioral and faunal transitions described above took place (Figs. 1 and 2). A structurally controlled southward slope and faulting episodes that created rift sub-basins have been recognized for some time in the southern Kenya rift (*18*). We thus reasoned that a drill core in the Koora basin adjacent to and directly downstream from the Olorgesailie basin could recover

Table 1. Comparison of Acheulean technology [typified by handaxes and other large cutting tools (LCTs)] and MSA technology. Behavioral and environmental comparison includes lithic source access and rock transport, pigment use, and environment evidence based on observations in the Olorgesailie basin (*6*–*8*, *34*), located 22 to 24 km from the OLO12-1A drilling site. Predicted insolation dynamics (high or low climate variability) based on (*5*).

Comparisons (Olorgesailie basin)	Acheulean Olorgesailie Fm. (1.2 Ma to 499 ka ago)	MSA lower Oltulelei Fm. (~320 to 295 ka ago)
Artifact/tool size	Large tools, LCTs dominant	Smaller, diversified tools
Focus of lithic source access	Local volcanic rocks, coarse, and fine-grain (98%)	Fine-grain rocks (e.g., obsidian, chert, and fine-grain local volcanics)
Stone transport distances	No more than 5 km	Obsidian transfer: 25 to 95 km, from multiple directions
Altered and used pigments	No	Yes
Depositional regime (horst-graben formation)	Stable, aggrading system (lake/fluvial/floodplain)	Highly dynamic landscape (sub-basin cutting-and-filling)
East Africa insolation (precipitation dynamics)	Alternating high-low climate variability	Sustained period of strong climate variability

sediments preserving high-resolution environmental data for the critical time window missing in the north. The present-day Koora basin is an up to 6-km-wide, 40-km-long graben bounded by ~1-million-year-old (Ma) horst blocks of 50- to 150-m height above valley surface. The basin is filled with a sedimentary sequence that was drilled in its northernmost location, closest to Olorgesailie basin outcrops. We note that the Olorgesailie and Koora basins had demonstrable, although periodic, hydrological, and paleoenvironmental connections over time (Fig. 2), which facilitates relating the core environmental records to the archeological and paleontological evidence from Olorgesailie.

An age model presented previously by our research team for the core (*19*) provides the most precisely dated environmental record covering the past 1 Ma in East Africa. The 139-m-long core spans the period from ~1084 ± 4 ka to 83 ± 3 ka old based on the age model constrained by ^{40}Ar-^{39}Ar ages on 22 intercalated tephra layers and the Brunhes-Matuyama magnetic reversal (Fig. 1E, fig. S2, and text S1) (*19*, *20*). In this study, we examine how spatially localized data from the core can be connected to larger spatial scales of the regional environment and to the archeological and faunal evidence from the adjacent Olorgesailie basin.

We emphasize that the core data concerning vegetation, lithology, and hydrology provide evidence on a variety of spatial scales ranging from local to regional. The archeological data to which we link the core records also reflect wider spatial scales beyond the excavations themselves. Lithic sources used by the Olorgesailie hominins document an expansion of resource acquisition substantially larger than the Olorgesailie basin itself (*6*). Obsidian used in MSA technology was transported from multiple volcanic outcrop sources located in different directions over distances of minimally 25 to 95 km from Olorgesailie, in contrast with ≤5-km distance of stone transport typical of the Acheulean tool assemblages (Table 1) (*6*, *7*). Integrating these data and observations with evidence of regional tectonism and landscape partitioning provides a framework for connecting, at high geochronological resolution, the sequence of changing resource landscapes with the critical transitions in hominin behavior and fauna.

Data compilations on human foraging behavior, which include more than 150 hunter-gatherer societies from low-latitude environments, show that diet, foraging range, group mobility, and size, among other adaptive characteristics, are systematically related to environmental setting (*21*–*23*). According to these ethnographic observations, hunter-gatherers tend to increase their investment in technology, expand their range of resource acquisition, and rely on distant social alliances and exchange networks in situations of heightened resource unpredictability and risk (*23*, *24*). Given that these responses in modern human foragers have parallels in the archeological innovations of the Olorgesailie MSA (*6*, *7*), we examined the core record to test the hypothesis that decreased resource predictability could have been a factor in the early appearance of MSA adaptations in the southern Kenya rift. The specific question we address is whether MSA behaviors replaced the Acheulean in this region during a period of increased resource fluctuation, an ecological factor that could have more broadly shaped the emergence of observed adaptive responses of *H. sapiens* foragers.

RESULTS

The sediment core was recovered in the Koora basin at a location ~24 km south of the Olorgesailie outcrops that preserve evidence of the large shifts in hominin behavior and faunal communities discussed above. The core's trachytic basement rock is overlain by a complex succession of diatomaceous, carbonate-rich, siliciclastic, and volcaniclastic fluvial and mostly lacustrine sediments, with multiple intervals of pedogenic alteration (Fig. 2). Our analyses have yielded environmental data spanning most of the past 1 Ma, including, particularly, high-resolution data for the temporal window of interest between 500 and 300 ka ago. We focused on exploring changes in the availability of ecological resources by reconstructing vegetation dynamics, paleohydrology, and hydroclimatic signals.

Ecological indicators

The core datasets allow us to track the past availability of freshwater on the landscape, which is a limiting factor for most mammal species in eastern Africa and therefore strongly affects populations in the area (*25*). To examine past changes in water supply, we used a set of paleohydrological proxies including sediment stratigraphy, diatom assemblage data (transfer functions), x-ray fluorescence (XRF) elemental profiles, and x-ray diffraction (XRD) minerology (Fig. 3A). Diatom-based records of electrical conductivity (EC) and planktonic versus benthic taxa (diatom CA axis 1) were used to reconstruct changes in Koora basin salinity and relative lake depth (*26*), respectively (Fig. 3A and fig. S3), thus reflecting the availability of potable water contained in a lake source. We integrate these paleohydrological records with evidence of 30 paleosols, each broadly estimated to represent subaerial exposure of ~50 to ~5000 years duration on the basis of soil maturity and structure [see Materials and Methods; (*19*)], which together indicate repeated lake-land transitions. Sedimentary structures such as burrows that formed in subaerially exposed sediments

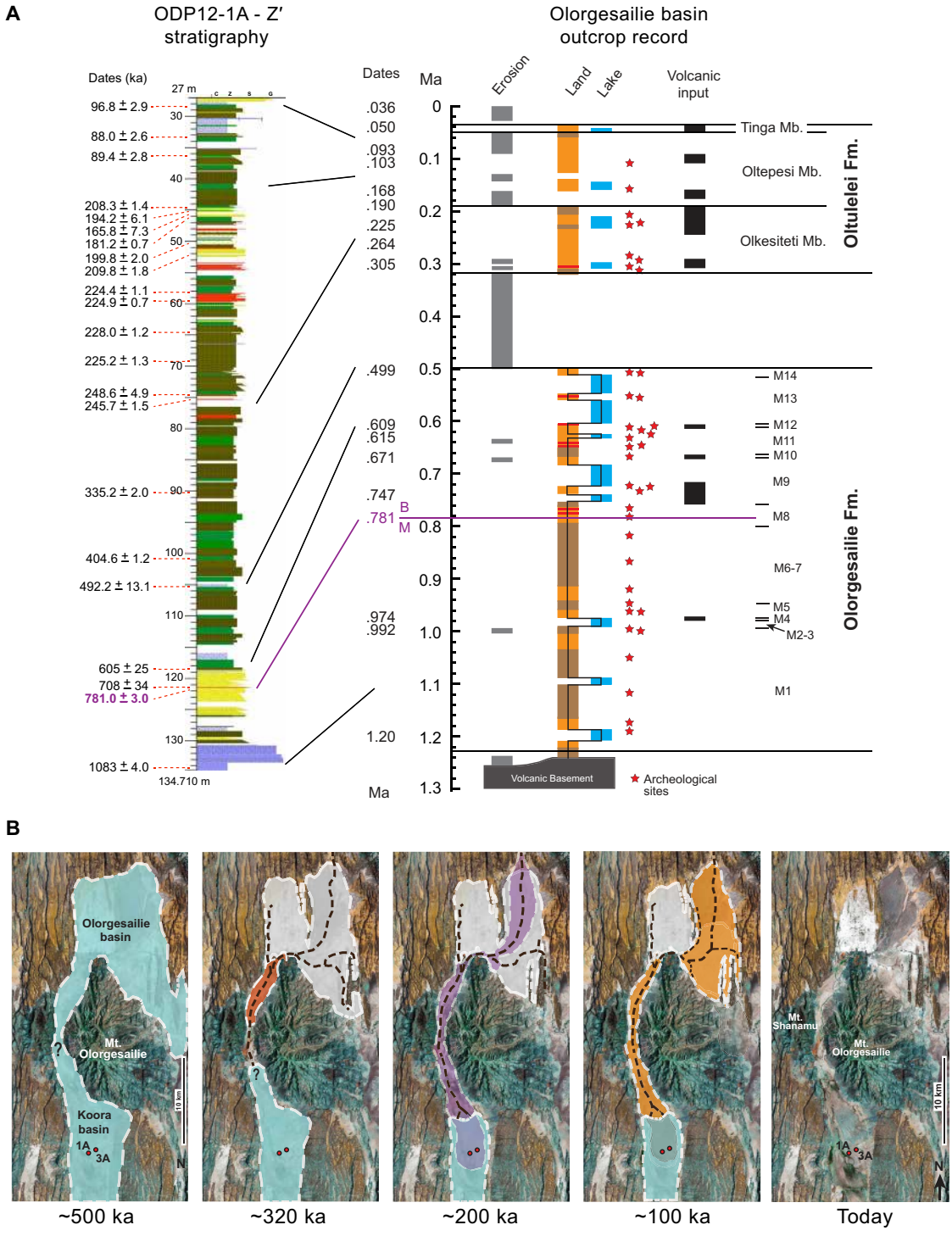

Fig. 2. Stratigraphic and paleohydrologic relationships between the Koora basin, where the ODP-OLO12-1A drill core was obtained (Fig. 1), and the Olorgesailie basin, where the transitions in Acheulean-MSA behavior and mammalian fauna are recorded. (**A**) Correlation between OLO12-1A *z*-prime core stratigraphy and the Olorgesailie basin outcrop record, based on dates in (*7*, *8*, *19*). The core's stratigraphic column is corrected for rapid and instantaneous deposits with thick volcanoclastic layers (red color) and event deposits removed. The overall *z*-prime core thickness is therefore lower than that of the recovered core; see (*19*). Outcrop Land color code: orange, aggrading sediment; brown, stable land surface; red, burned zone. (**B**) Hypothesized reconstruction of basin history and drainage relationships of the Olorgesailie and Koora basins from 500 ka ago to present. The sequential maps show the connections between the two basins, based on sediment correlations and tephra dates, and illustrate increasing compartmentalization of this part of the southern Kenya rift over the past 500 ka (*34*). This reconstruction conforms to the present-day topography; the spatial extent of the Koora basin paleolake is approximate. Question marks denote uncertainties in lake extent in the northern Koora basin. Color code: blue, lake; white, eroding outcrops of the Olorgesailie Fm.; red-orange, major paleosol (base of Olkesiteti Mb., Oltulelei Fm.); purple, major volcaniclastic influx (Olkesiteti Mb, Oltulelei Fm.); orange, volcaniclastics plus fluvial siliciclastic sediments (Oltepesi Mb., Oltulelei Fm.). Red dots in the Koora basin mark the locations of drill cores.

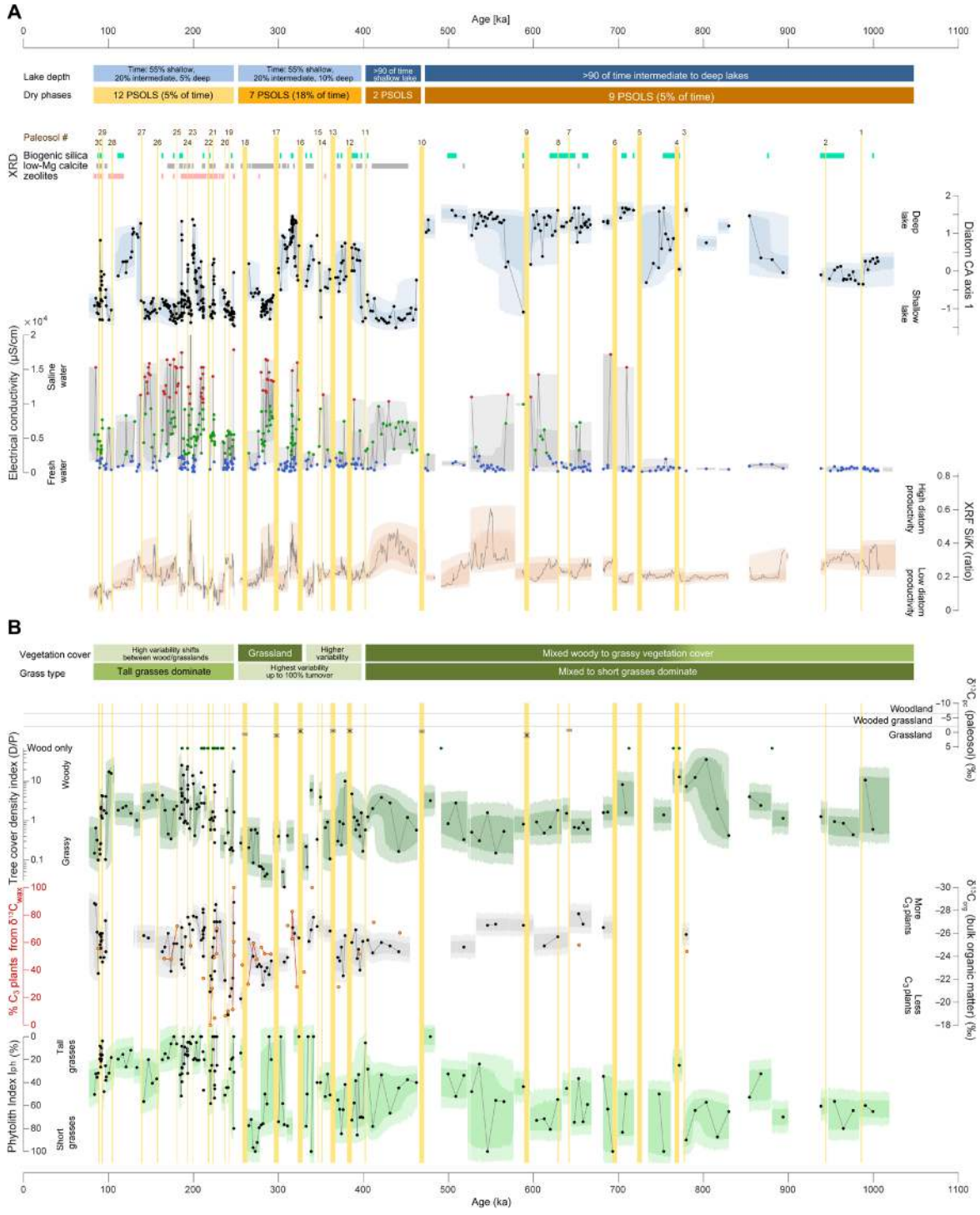

Fig. 3. Paleoenvironmental data from core ODP-OLO12-1A. Colored horizontal bars summarize intervals of similar paleoenvironmental conditions; darker to lighter colors represent lower to higher variability intervals. Vertical yellow bars denote paleosols (PSOLS), indicating lake desiccation. (**A**) Water availability data: XRD shows major mineral groups (zeolites: predominantly analcime and phillipsite). Correspondence analysis (CA) scores of diatom assemblage data indicate fluctuations in lake water depth. EC of paleolake waters are derived from a diatom transfer function (blue, fresh; green, brackish; red, saline; 2500 µS/cm assumed limit of potable water for humans). Ratio of silica and potassium counts from XRF analysis shows five-point moving average; high (low) values indicate high (low) diatom productivity (text S3) (*88*). (**B**) Vegetation dynamics data: Stable carbon isotope values of carbonate nodules ($\delta^{13}C_{pc}$) from paleosols; vegetation classes from (*89*). Tree cover density index (D/P) of phytolith assemblage data (*30*): higher values indicate dense woody cover; green dots denote absence of grass phytoliths. Stable isotope values of bulk sedimentary organic matter ($\delta^{13}C_{org}$; black) and proportion of C_3 versus C_4 plants from plant leaf wax isotopes ($\delta^{13}C_{wax}$; red). Phytolith index (Iph) from grass phytolith data indicate proportion of short (Chloridoideae) versus tall (Panicoideae) grasses (*29*). All datasets are plotted at their median age. Dots denote single data points; envelopes reflect 68% (dark) and 95% (light) confidence intervals (*19*). Continuity of data and uncertainty envelopes are interrupted at hiatuses, core gaps, and measurement gaps.

document periods of lowered water table down to several meters below the emergent land surface (table S2 and text S2). We measured the carbon isotopic composition of pedogenic carbonates ($\delta^{13}C_{pc}$) from the paleosols and obtained values of between −1.28 and 2.03 per mil (‰) (average 0.03‰), which consistently indicate local C_4 grasslands during subaerial intervals (Fig. 3B). On the basis of the combined evidence, we conclude that each emergent land surface represents a period of marked lake regression and local to lake-basin-wide desiccation. Multiple lithological transitions between lacustrine sediments and paleosols throughout the core can thus be explained by marked variations in water supply to the Koora basin.

Vegetation is also a critical resource for many mammal species, especially herbivores, and a primary determinant of habitat, dietary, and foraging opportunities. We reconstructed vegetation cover and composition on local to regional scales by using carbon isotopes of leaf waxes, bulk organic matter, and pedogenic carbonates ($\delta^{13}C_{wax}$, $\delta^{13}C_{org}$, and $\delta^{13}C_{pc}$) and also phytolith assemblage data (Fig. 3B) (see Materials and Methods). The carbon isotope data are interpreted in terms of the proportion C_3 to C_4 plants, with C_4 plants, mainly grasses, having higher water use efficiency adapted to arid conditions (*27*).

These carbon isotope–based proxies were necessarily obtained from different lithologies; they thus preserve vegetation signals representing different yet overlapping time periods and varied spatial scales. Whereas the $\delta^{13}C$ signature of pedogenic carbonates reflects only a localized signal preserved in dry and exposed land surfaces lacking sediment input (i.e., no aggradation), these conditions resulted in poor preservation of leaf waxes and organic matter. Thus, leaf wax and bulk organic $\delta^{13}C$ samples were extracted from lacustrine sediments. The bulk organic $\delta^{13}C$ measurements contain a mixed signal of basin-scale terrestrial vegetation and aquatic biomass (e.g., algae) originating from the lake itself. The source area of bulk organic $\delta^{13}C$ is smaller than that of the leaf wax $\delta^{13}C$ samples because the transport of waxes is partly fluvial and partly aeolian (wax aerosols), and the latter can result in long-distance dispersal. Leaf waxes are primarily produced by terrestrial vascular plants; therefore, the sediment leaf wax $\delta^{13}C$ signal reflects the past C_3/C_4 plant composition from the Koora basin and its catchment.

The phytolith data also record vegetation signals on local (during dry phases) to regional (fluvial transport during wet phases) scales. An advantage of including phytolith morphotypes in our analysis is that they can be resolved taxonomically (*28*, *29*). From the phytolith assemblages, we determined the tree cover density index (D/P) and the phytolith index (Iph). The D/P ratio is the proportion of woody dicotyledons (D) over grasses (Poaceae, P), which we use to estimate woody plant cover on the paleolandscape (*30*, *31*). The Iph records the proportion of short (Chloridoideae) and tall grasses (Panicoideae) in savanna ecosystems, with values of >20 to 40% indicating short-grass dominance (*29*, *31*). In Africa today, areas of higher water availability generally favor woody vegetation and/or tall grasses (Panicoideae), whereas arid conditions favor short grasses (Chloridoideae) (*29*), which allows us to link past vegetation composition with paleohydrology.

A shift in ecological resources

The core record exhibits mostly subdued variability in both the lacustrine and terrestrial datasets during its first ~500 ka , followed by a 400-ka-long interval of marked variability and ecological disruptions (Fig. 3). The division of the record into two major variability phases is also illustrated by a doubling of dry intervals of emergent land surface (n = 9 paleosols before 500 ka ago versus 20 paleosols after). Overall, the proxy data contain only weak orbital signals (11 to 17% of the variance), dominated by the 100-ka eccentricity period in the lake depth reconstruction (diatom CA axis 1), the XRF Si/K ratio, and D/P tree cover index (Fig. 4 and fig. S4).

Between ~1 Ma and 470 ± 15 ka ago, intermediate to deep freshwater lakes prevailed in the Koora basin as inferred from the diatom CA axis 1 and EC reconstruction (median EC <800 µS/cm; Fig. 3A). These lake phases were interrupted by nine emergent land phases represented by paleosols that lasted for ~1000 to ~5000 years (*19*). Most of these dry phases occurred between 780 and 590 ka ago. However, the combined duration of all nine dry episodes represents only ~5% of this 530-ka-long period based on the age model (*19*). The evidence indicates that freshwater was generally available in the Koora basin (Fig. 3A) during the period when Acheulean toolmakers were active at Olorgesailie.

A reliable freshwater supply would have sustained the predominantly water-dependent fauna of the region up to ~470 ka ago (Fig. 1D). Before the major faunal and archeological transitions (i.e., before 500 ka ago), intermediate values of the D/P tree cover index with a median of 1 (range, 0.2 to 36; Fig. 3B and fig. S5) indicate a mix of woody and grassy vegetation typical for African tall and short grass savannas (*29*). The stable isotope record for this interval shows depleted $\delta^{13}C_{org}$ values, ranging from −24.9 to −27.7‰ (average, −26.4‰), which are typical for C_3-dominated vegetation consistent with the D/P values of mixed vegetation. Coupled with evidence of intermediate-deep freshwater lakes, this vegetation composition points to relatively high moisture levels during the first 500 ka of the record. However, unexpectedly, we determine high Iph values with a median of ~60%, indicative of the concurrent predominance of short grasses (Chloridoideae; Fig. 3B), which typically prevail in arid grasslands and conditions of low soil moisture (*29*). The concurrent predominance of short grasses suggests that vegetation was influenced by factors beyond water availability (precipitation).

The prolonged freshwater period was disrupted at 470 ± 15 ka ago, initially by a ~ 5-ka dry episode followed by >60-ka interval of shallow and saline lake conditions (median EC, >5500 µS/cm; Fig. 3A), marking the transition to an interval of high environmental variability. During the critical time window between 500 to 300 ka ago, eight intervals of desiccation are recorded as paleosols, five of which are estimated to have lasted for ~5 ka each (Fig. 3). The intervals between these dry phases are approximately 68, 16, 19.5, 15, 5.5, 18, and 29 ka long, which conform partly with precessional frequencies and partly with nonorbital rhythms (fig. S4).

In concert with these more frequent wet-dry shifts, ecological resources began to fluctuate more widely by ~400 ka ago in both terrestrial and aquatic environments. Each of the lake phases during the critical window was distinct in terms of lake depth, salinity, diatom productivity, and composition (Si/K ratio; Fig. 3A and fig. S4), Together with the more frequent subaerial intervals, these variable lake conditions point to large fluctuations in lake level and highly variable moisture supply. Between ~400 ± 5 ka and 320 ± 7 ka ago, the D/P tree cover index (0.1 to 10; median, 0.7) reveals rapid shifts between woody vegetation and grassland in line with varying water availability (Fig. 3B and fig. S5), consistent with assemblage-based ecological variability (fig. S6). This varying woody plant cover is also evident in larger fluctuations of $\delta^{13}C_{org}$ (−27.4 to −22.3‰) and $\delta^{13}C_{wax}$ (−34.5 to −22.9 ‰), suggesting shifts between C_3-dominated (100%)

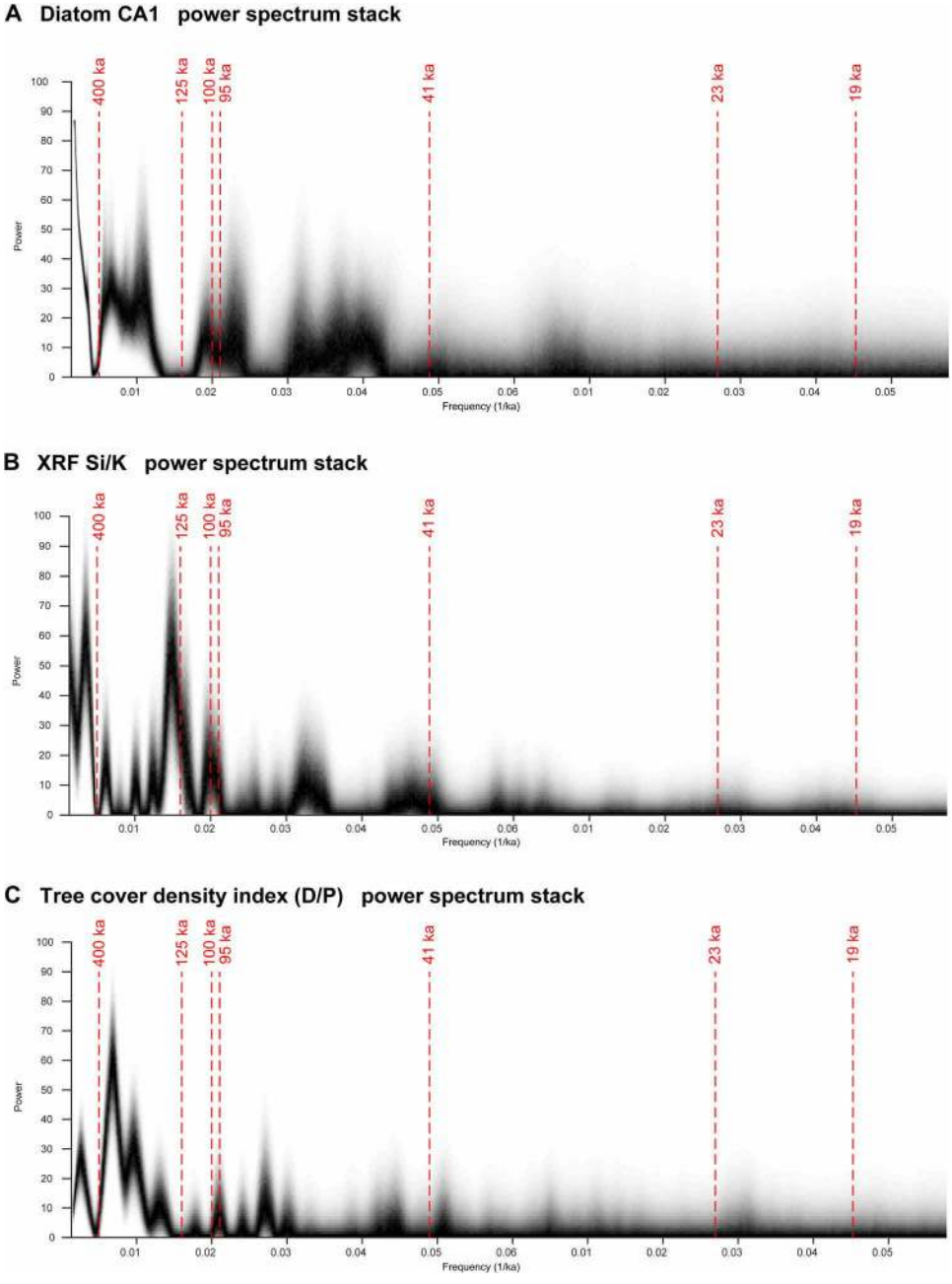

Fig. 4. Time-series (power spectrum) analyses on ODP-OLO12-1A environmental indicator (proxy) records. Lomb-Scargle spectra for (**A**) the diatom CA1 axis, an indicator for lake depth, (**B**) the XRF Si/K ratio, an indicator of paleohydrology, and (**C**) the phytolith D/P index, an indicator of paleovegetation and tree cover. Orbital periods (400, 100, 41, and 23 to 19 ka) are shown with red dashed lines. Spectral analysis was used to explore orbital variability within the various time series, taking into account the uncertainty of the age model (see Materials and Methods). Darker colors represent spectral powers of the data that are more consistent across the full age model. Orbital variability is present but subdued in these records: The percentage of total variance occurring at orbital periods is only 11% in the diatom CA1 record (8% eccentricity, 2% obliquity, and 1% precessional periods), 17% in the XRF Si/K time series (8% eccentricity, 7% obliquity, and 1% precessional periods), and 16% in the phytolith D/P tree cover record (9% eccentricity, 3% obliquity, and 4% precessional periods). Records are shown in comparison with orbital cycles in fig. S4.

and C_4-dominated (~70%) vegetation. The grassland composition as inferred by the Iph implies pronounced variation in tall- and short-grass dominance and complete turnover between these two grassland types after 350 ± 8 ka ago (Fig. 3B). From ~330 to ~250 ka ago, the Koora basin was apparently dominated by open grassland vegetation; few phytoliths of woody plants in this interval result in a low median D/P index of 0.15. These grasslands were either characterized by tall- or short-grass abundance but rarely of mixed composition.

The Olorgesailie Acheulean-to-MSA transition and the major faunal turnover thus coincided with the onset of an ecological landscape characterized by decreased reliability of potable water and increased variability of grassland vegetation-type beginning ~400 ka ago.

The shift from megagrazers to a predominance of smaller-bodied herbivores, with a higher proportion of browsers and mixed feeders, suggests that change in the mammal community favored organisms that could adjust to diverse and/or fluctuating vegetation and dietary resources (Fig. 1D). In addition, the more water-independent mammal taxa present in the fauna by at least 320 to 300 ka ago in the southern Kenya rift would have been more resilient to erratic freshwater availability.

Beginning ~250 ka ago, after these transitions occurred, the phytolith data indicate a shift toward tall grass dominance (median Iph, <20%) and the return of woody plants but with highly varying density. This vegetation change is also recorded by $\delta^{13}C_{wax}$, which exhibits its overall largest fluctuations (between −32.9 and −18.4‰), thus suggesting complete turnover between C_3 and C_4 plant dominance (Fig. 3B and fig. S5). Frequent ecological disruptions continued based on the recurrence of short dry intervals (n = 12, after 250 ka ago), strongly fluctuating lake depth, and more frequent saline lake conditions (Fig. 3A).

DISCUSSION

What factors could have led to the transitions in water and vegetation resources, the loss of megagrazers, and the replacement of Acheulean by MSA behaviors? Although orbitally paced climate variability is well documented in many East African paleoclimate records (*1*–*5*), evidence for orbital cyclicity in our core data is weak compared to the large, abrupt, and increasingly frequent landscape changes that we document. Our analyses show that rainfall variations during the past 1 Ma were influenced by orbital pacing, mainly the eccentricity cycle, but temporal changes in water availability and vegetation as recorded in the core cannot solely be explained by orbital forcing. Millennial-scale climate variations have been demonstrated in Northern Hemisphere mid-Pleistocene records [e.g., (*32*, *33*)], but our indicator records at the current sampling resolution have not yet revealed this variability or temporal correlation with events documented at higher latitudes. The episodic prevalence of tall grasses (Fig. 3B; Iph), furthermore, is inconsistent with progressive aridity, another prominent hypothesis often invoked to explain hominin evolutionary change. By focusing on ecological resources rather than climate alone, our study suggests that a combination of geological, climatic, and ecological factors directly influenced fundamental shifts in hominin and faunal adaptations in the southern Kenya rift.

Previous geological observations document extensive faulting throughout the region after ~500 ka ago, manifested in the deep erosion of Olorgesailie Fm. outcrops to the north between ~499 and ~320 ka ago, and by drag-faulted sedimentary units that onlap horst walls after 499 ka ago at Olorgesailie and after 397 ka ago at Lainyamok to the southwest (*7*, *16*, *18*, *34*). Increased volcano-tectonic activity is further indicated by an abrupt, nearly twofold rise in sedimentation rate and increased volcanic tephra input in the Koora basin beginning ~400 ka ago (fig. S7) (*19*). One consequence of this tectonism was increased topographic relief and basin compartmentalization throughout the region (Fig. 1C and Fig. 2) (*35*). Tectonic development of the Koora basin's graben morphology (Fig. 1, B and C) over time would have resulted in amplified lake level fluctuations due to higher sensitivity of graben-shaped lakes to changing moisture supply (*36*).

As a result, spatial heterogeneity in runoff, soil moisture, water availability, and woody/grassy vegetation proportions was accentuated, with basins of varying size and morphology potentially developing different sensitivities and divergent resource landscapes in response to climate variations. These interactions may account for contrasting environmental histories apparent in the adjacent Magadi and Koora basins. The Magadi drill core provides the only other relatively high-resolution environmental sequence in the region relevant to the past 1 Ma. Its vegetation record is interpreted as evidence of progressive aridification (*37*), whereas the higher-resolution record presented here shows increased tall-grass dominance, mixed woody/grassy vegetation, and fluctuations in C_3 vegetation in the interval from 500 to 300 ka ago and after (fig. S8). This comparison indicates that, during the past 500,000 years, distinct ecological zones and resource landscapes developed over a distance of less than 20 km between the two rift basins (Fig. 1B). According to the relevant archeological data, distances of MSA obsidian transport were minimally ~25 to 95 km as straight-line measures, which further suggest that hominin foraging ranges and potential interactions among groups encompassed diverse resource landscapes from the southern to the central Kenya rift (*6*). This observation links the hominin and faunal transitions in southern Kenya with spatial heterogeneity in ecological resources in addition to the temporal variability shown here.

We note that the development of accentuated horst-graben topography also would have dissected and diminished the spatial continuity of grazing landscapes. Persistent high grazing pressure is known to transform broad areas of moist, wooded, and tall grass habitats into extensive short-grass grazing lawns (*38*–*40*). From ~1.0 Ma ago until the faunal turnover after 500 ka ago, the megagrazers of the southern Kenya rift had craniodental specializations and estimated body masses up to ~20% (e.g., the zebra *Equus oldowayensis*) to 400% (e.g., the baboon *Theropithecus oswaldi*) larger than their modern counterparts (*41*, *42*), which together suggests a unique grazing community that had the capacity to establish and sustain short-grass grazing lawns despite the prevailing moist conditions (*39*, *40*).

We propose that the megagrazer decline and emergence of a different suite of mammal species was a response to a more spatially fragmented and fluctuating resource base, which began ~400 ka ago and thus within the critical window of faunal and archeological change (Fig. 5). A combination of factors including accentuated topographic relief, climate variability, hydrological subdivision of the region, and fragmentation of vegetation types could have created an interactive cascade that diminished megagrazer populations in the region. This would have put specialized grazers dependent on predictable short-grass and freshwater availability at a disadvantage relative to mixed feeders and water-independent browsers, which increased between ~400 and 320 ka ago (Fig. 1D) (*8*). Small obsidian points with retouched bases recovered from Olorgesailie archeological sites are suggestive of projectile armaments dated ~320 to 307 ka ago (*6*) and thus potentially indicate hominin predation as a possible influence on herbivore turnover in this region. Since the definitive loss of megagrazer species in the region is recorded at 397 to 334 ka ago [Lainyamok fauna; (*8*, *43*)], the Olorgesailie MSA stone points could, however, reflect a technological innovation for hunting smaller prey following the loss of megagrazer species (see Fig. 1D).

We further suggest that compartmentalizing of the southern Kenya rift into horst/graben-delimited basins with quasi-independent resource dynamics also favored the transition to MSA behavior. Even as mammalian populations experienced increased fragmentation of vegetation types due to topographic partitioning of the landscape, evidence of widespread obsidian exchange networks by ~320 to 295 ka ago (*6*, *8*) implies that the MSA hominin groups actually became more connected across the larger region. This response was potentially

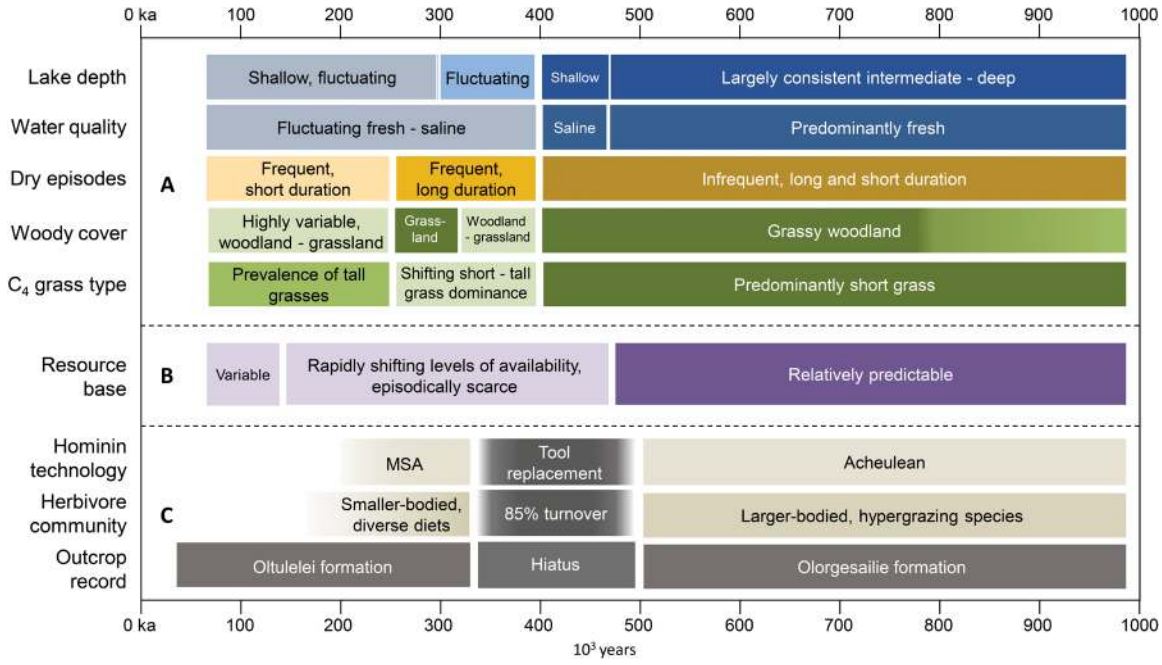

Fig. 5. Transitions in resource dynamics, hominin behavior, and mammalian fauna over time based on the OLO12-1A drill core and Olorgesailie outcrop data. (**A**) Water availability and vegetation dynamics based on Fig. 3 datasets (see text). Darker bars reflect relatively consistent resources, lighter colors more variable resources. Intermediate-to-deep lake conditions ~938 to 830 ka ago are based on lower-resolution data due to core gaps (table S4). (**B**) Change in resource base availability and predictability based on the synthesis in (A). The horizontal bars in (A) and (B) describe dominant inferred patterns for each time period of the core; the transitions are not typically abrupt. (**C**) Major transitions in hominin behavior and the herbivore community based on outcrop records of the southern Kenya rift. These transitions took place during the erosional hiatus between 500 and 320 ka ago. The marked shift from reliable to variable resource landscapes beginning ~400 ka ago in the adjacent Koora record (fig. S9) occurred within the interval of the Olorgesailie erosional hiatus and the major transitions.

critical to their evolutionary success in the changed resource regime. We hypothesize that MSA technological innovations and distant resource exchange, sustained by symbolic communication, reflect an ability to respond to increased instability in resource landscapes through risk mitigation, an adaptive strategy ultimately characteristic of human foragers today (*23*, *24*).

On the basis of our study, concurrent reshaping of hominin behavior and the faunal community can be understood as distinctive responses to similar ecological stresses. We conclude that although MSA adaptations may have originated elsewhere, they took hold in the southern Kenya rift between 400 and 320 ka ago as a result of heterogeneity in selective conditions induced by the marked shift to a temporally and spatially varied and less predictable resource landscape, favoring hominin populations with resilient adaptations. Early evidence of this response suggests that fundamental aspects of human adaptability had emerged by the time of our species' African origin.

Our study prompts a wide range of questions for future investigation. We do not address here the continent-wide demise of the Acheulean and its replacement by the MSA but offer a resource landscape hypothesis that could be tested in other parts of Africa. Last records of the Acheulean occurred at various times in other African regions [e.g., (*44*)], later than in the southern Kenya rift. The onset of the MSA, furthermore, is recorded at varying times in different places, and MSA sites across the continent are associated with diverse environmental settings (*14*, *45*). In our study, the oldest documented transition from Acheulean to MSA in eastern Africa occurred in the context of repeated environmental disruptions. The hypothesis that we present, which is limited to a conjunction of factors in the southern Kenya rift, should be examined elsewhere to see whether the MSA flourished at the expense of the Acheulean under similar circumstances of ecological disturbance. We recognize, however, that once MSA behaviors evolved, the adaptive flexibility they conferred would have been advantageous and sustained in other locations where the MSA spread, including in relatively stable habitats.

Integration of resource dynamics with regional tectonic and ecological history, as exemplified by our study, also suggests a new direction in the search for causal processes that shaped human evolution. Evolutionary adaptation entails not only the origin of behavioral variations (*7*) but also their increase within a population and spread across a wider geographic area. Studies of how environment may initiate evolution, therefore, need to further address the processes that underlie adaptive change rather than assume, for example, that correlations between evolution and either aridity, moisture, or variability provide a useful explanatory hypothesis for any given change (*5*). Robust ecological theory as applied to human hunter-gatherers and mammal herbivores provided the framework for investigating the potential environmental influences on the hominin and faunal adaptations described here. We intend this approach to be useful in motivating future research on how environmental dynamics may have led to critical transitions in human evolution.

MATERIALS AND METHODS

Bayesian age model (C.B.K.)

To constrain the absolute chronology of the ODP-OLO12-1A core, a high-resolution age-depth model (fig. S2) was constructed using a

Bayesian stochastic sampling approach to combine quantitative age constraints from Ar-Ar geochronology, semiquantitative minimum estimates for the duration of observed exposure surfaces (depositional hiatuses), and the absolute constraint of stratigraphic superposition. As described in (*19*), this Markov chain Monte Carlo model uses the Metropolis algorithm to estimate the posterior age distribution for each centimeter of core depth. At each step of the Markov chain, the previous age-depth model is perturbed by a symmetric Gaussian proposal distribution, checked for stratigraphic superposition, and evaluated against the combined quantitative constraints. Since adjacent proposals are highly correlated, this model was run with a burn-in of 20,000,000 steps, and a sieved stationary distribution collected over the subsequent 500,000,000 steps of the Markov chain.

Age and proxy uncertainty analysis (S.R. and Y.G.)

Paleoenvironmental proxy data were translated into the time domain considering both proxy and age model uncertainties by calculating uncertainty envelopes (shown in Fig. 3). Envelope width along the time direction (*x* axis) represents absolute age uncertainty based on the age model. Envelope height in the proxy direction (*y* axis) represents the analytical uncertainty of the proxy dataset. These uncertainty envelopes were generated by using the full age model output: For each proxy data point, its *z*-prime depth was assigned to the complete corresponding sieved age distribution (n = 25,000) of the full age model at sample depth. (fig. S2 shows the age model uncertainties on the *z*-prime depth scale.) The analytical uncertainties of the proxy data were assumed to have a normal distribution. These two individual uncertainties, in time domain (age model) and proxy domain (analytical uncertainty), were used to generate two-dimensional histograms for each data point. The obtained probabilities were then combined to composite probabilities per continuous section of the dataset. The environmental proxy records were treated as discontinuous sections wherever the record was interrupted either by a paleosol occurrence (hiatuses), by absence of core recovery (depth gaps), or by measurement gaps. A conservative discontinuity criterion was further applied if neighboring data points were too remotely spaced, either in time axis (threshold of 20 ka) or in the depth axis (threshold of 10 m). For each obtained continuous time interval, the obtained probability densities of individual data points were merged into a composite probability. The resulting 68 and 95% confidence envelopes were ultimately extracted from the obtained composite probability distributions. All the processing was undertaken using MATLAB (*46*).

Spectral analysis (S.R. and P.d.M.)

To analyze orbital variability within the time series, Lomb-Scargle power spectra were calculated because of their ability to work with unevenly spaced data as represented in this drill core. The absolute uncertainty of the age model was included by converting the proxy data into the time domain for each individual *z*-prime–time distribution of the full age model (n = 25,000). Lomb-Scargle power spectra were then calculated for each of the resulting time series of a specific proxy (Fig. 4). Individual spectra (n = 25,000) were stacked to create one representative spectral power density plot. This density plot shows the frequency spectrum of the proxy data, taking into account time uncertainty in the full age model. Higher densities in the stacked spectrum denote spectral powers, which are consistent across the full age model.

Diatoms (R.B.O.)

Diatom samples were collected every 30 cm and where facies changed, with sampling intervals reduced to 10 cm in relatively pure diatomites. Subsequent resampling of diatomaceous deposits was carried out to reduce intervals for these sediments to 10 to 12 cm. Samples were weighed and placed in a Calgon solution to assist dispersion. After washing with distilled water, 10% HCl was added to remove carbonates followed by further washing. Subsequently, 30% H_2O_2 was added, followed by washing. In the last stage, a known number of microspheres (8 μm in diameter) were added to enable quantitative counting. Smear slides were prepared using Naphrax. A minimum of 400 diatoms were counted, except where diatoms were rare in which case all frustules were tallied. Diatoms were included in counts when more than half of a frustule was present. Apices were counted for fragmentary long thin fragile taxa. Diatoms were identified at ×1000 magnification with the supplementary aid of a LEO 1530 field-emission scanning electron microscope. Identifications used standard taxonomic works and, especially, Gasse (*47*, *48*). Correspondence analyses (CAs) were carried out using CANOCO 4.5 with taxa that formed ≥3% in at least two samples or ≥ 10% in at least one sample, included in analyses (n = 476). CA axis 1 tracks water depth, indicated by a high correlation with percentage of planktonic taxa, with negative values associated with abundant *Aulacoseira* spp. and rare *Stephanodiscus* (r = −0.959, P < 0.001) and positive values associated with benthic taxa (shallow). The percentage variance explained by CA axis 1 is 68%. Environmental reconstructions were performed using ERNIE software v. 1.2. EC for each sample (n = 476) was determined using the European Diatom Database (EDDI) "Combined Salinity Dataset", and "Locally weighted Weighted Averaging."

Phytoliths and pollen (R.K., R.D., and S.M.R.)

Two hundred seventy-two phytolith samples, 2 to 3 cm^3 in volume, were collected at 48-cm intervals with finer sampling at ±10-cm interval depending on core lithology. Samples were processed using a modified heavy liquid floatation (*49*) as outlined in (*50*): (i) dissolution of carbonates with HCL, (ii) oxidation of organic matter using HNO_3, (iii) heavy liquid floatation using Sodium Polytungstate at density of 2.4 g/cm^3, and (iv) gravitational removal of clay. The recovered fraction was mounted on microscope slides using Entellan New medium. Freshly mounted slides were viewed under an Olympus BX52 microscope at ×400 magnification for three-dimensional observation and counting. Because most samples had low phytolith abundances, phytoliths >5 μm in diameter in each sample were counted and classified with aim of attaining a minimum of 200 grass short silica cells (GSSCs) to acquire a statistically robust dataset. Identification and classification of phytoliths largely followed the International Code of Phytoliths Nomenclature (*51*) with refined GSSCs classification based on (*52*–*54*) and with further consultation of other published studies (*28*, *50*, *55*–*70*). Phytolith data interpretation was based on two approaches. First, abundance diagrams generated using Tilia program (*71*) showed variation in phytolith assemblages throughout the core, which provided information about vegetation structure through time (*50*). Second, phytolith indices were computed to determine changes in vegetation composition and climatic conditions. Two phytolith indices were calculated: The D/P tree cover index is the ratio of woody dicotyledons to all grasses and indicates changes in tree cover density through time (n = 218) (*30*). The index was computed by dividing rough globular phytoliths with the sum of Poaceae phytoliths from the subfamilies Panicoideae,

Chloridoideae, Arundinoideae, and Aristidoideae (dumbbell, cross, saddle, point-shaped, and fan-shaped types). The Phytolith index (Iph) presents the relative proportion of Chloridoideae (aridity affinity C_4 short grasses) versus Panicoideae (moist affinity C_{3+4} tall grasses) and was used to investigate temporal changes in this water availability indicator (n = 183). The Iph was computed as the ratio of Chloridoideae (saddle morphotype) to the sum of Chloridoideae and Panicoideae (saddle, cross, and dumbbell morphotypes) (*29*). Cores were also sampled for pollen: Samples were processed at Ghent University in Belgium following standard palynological procedure for concentrating pollen grains (*72*). Slides mounted for pollen counts were examined at the National Museums of Kenya, Department of Earth Sciences. Pollen was investigated using a Leitz microscope at ×400. Pollen preservation was very poor. Most slides had no pollen, but in rare cases, one or two grains were observed. Poor preservation might have been influenced by oxidation, high temperature, and low organic matter content, among other external factors.

Identification of hiatuses and paleosols (E.J.B.)

Thirty hiatuses marked by paleosols occur in core OLO12-1A and range from weakly to moderately develop. These paleosols are identified by diagnostic soil features such as bioturbation, soil peds, horizonation, and pedogenic carbonate. The top of each paleosol was identified by a lithologic change and loss of ped structure, and the bottom of each paleosol by the return of identifiable parent material lithology such as laminated lacustrine sediments. The presence or absence and degree of development of these features allows for classification of the paleosols using U.S. Department of Agriculture Soil Taxonomy as paleo-Entisols, paleo-Inceptisols, and paleo-Vertisols (*73*). The core ODP-OLO12-1A Entisols are very weakly developed soils with little or no evidence of soil horizons, and they often contain relict bedding. The Inceptisols are more strongly developed than Entisols with soil horizonation and ped formation but lack distinguishing features that would allow them to be classified as another soil order. The Vertisols are clay-rich soils with cracks, pedogenic slickensides, and other vertic features that form as a result of shrinking and swelling of clays during wetting and drying. These diagnostic features also allow for classification of these paleosols into a paleosol maturity index modified from (*74*). This paleosol maturity index can then be related to approximate the duration of pedogenesis as certain soil features form at different time scales. For additional discussion of the paleosol characterization and estimates of duration for the age modeling, see (*19*).

$\delta^{13}C_{wax}$ and $\delta^{13}C_{org}$ (J.M.R., R.L., K.U., and P.d.M.)

We measured the carbon isotopic composition of terrestrial leaf waxes (n = 37) following the protocol outlined in (*75*). Lipids, which include leaf waxes, were extracted from freeze-dried and homogenized bulk sediment using a DIONEX Accelerated Solvent Extractor 350 with dichloromethane:methanol (9:1). The lipids were separated into neutral and acid fractions over an aminopropylsilyl gel column using dichloromethane:isopropanol (2:1) and ether:acetic acid (24:1). The acids were methylated using acidified methanol of known isotopic composition, and the resulting fatty acid methyl ethers (FAMEs) were purified via silica gel column chromatography. Relative abundances of the FAMEs were quantified using an Agilent 6890 gas chromatograph (GC) equipped with a HP1-MS column (30 m by 0.25 mm by 0.25 μm) and flame ionization detector. Carbon isotopes were measured on an Agilent 6890 GC equipped with HP1-MS column (30 m by 0.25 mm by 0.10 μm) coupled to a Thermo Delta V Plus isotope ratio mass spectrometer (IRMS) with a reactor held at 1100°C at Brown University. The IRMS was run with CO_2 of known isotopic composition as the external standard for normalization to the Vienna PeeDee Belemnite (VPDB), and a FAME internal standard containing four homologs was measured every sixth injection to monitor instrument performance and drift. Repeated measurement of the internal standard yielded a standard deviation (1σ) of 0.20‰. Carbon isotope ratios were measured in duplicate on each sample with a mean intersample difference of 0.20‰. All carbon isotope measurements were corrected for the isotopic composition of the added methyl group, where $\delta^{13}C_{MeOH} = -36.5$‰. We also analyzed the carbon isotopic composition of bulk sedimentary organic matter ($\delta^{13}C_{org}$). The samples (n = 116) were acidified in 2 N hydrochloric acid (HCl) for 1 hour at 80°C to remove carbonate minerals. The acid-treated samples were rinsed in deionized water and centrifuged four times to remove excess HCl and were then lyophilized and homogenized before isotopic analysis. The $\delta^{13}C_{org}$ values were measured using a Carlo Erba Elemental Analyzer coupled to a Thermo Delta Plus IRMS. The analytical precision determined through replicate measurements of internal sediment standards was 0.14‰. All $\delta^{13}C$ values are reported relative to the VPDB standard.

$\delta^{13}C_{wax}$ primarily records changes in the relative abundance of plants using the C_3 photosynthetic pathway (trees, shrubs, and cool season grasses) versus plants using the C_4 photosynthetic pathway (warm season grasses and sedges) (*76*, *77*). To quantify the relative abundance of C_3 and C_4 vegetation, we used a two end-member mixing model that uses a $\delta^{13}C$ of n-C_{30} acids of −32.9‰ for the C_3 end member and a $\delta^{13}C$ of n-C_{30} acid of −19.0‰ for the C_4 end member based on wax isotope measurements from the Turkana Basin in northern Kenya (*78*). Measurements of the $\delta^{13}C$ of n-C_{28} and n-C_{30} acids from the Turkana Basin and various terrestrial plants (*79*) indicate negligible offsets between these homologs, allowing us to apply the end member $\delta^{13}C$ compositions from the n-C_{30} acids. Our use of −32.9‰ for the C_3 end member assumes that closed canopy forests, which can produce waxes with much more depleted $\delta^{13}C$ values (*80*, *81*), were not substantial contributors to the waxes in the core. This assumption is justified by the multiproxy data from our sediment core that indicates generally dry conditions through the past 1 Ma. The bulk organic matter in lake sediment derives from both internal and terrestrial sources, and its $\delta^{13}C$ records both aquatic carbon cycling and the $\delta^{13}C$ of terrestrial organic inputs (*82*), largely driven by C_3/C_4 plant abundance. Although we cannot determine the relative abundances of aquatic versus terrestrial organic matter within the bulk sedimentary organic matter in the ODP-OLO12-1A drill core, recent work has shown that the $\delta^{13}C_{org}$ of tropical lakes responds strongly to changes in C_3/C_4 plant abundance (*83*, *84*). We interpret the $\delta^{13}C_{org}$ in the ODP core to reflect both aquatic ecosystem carbon cycling and C_3/C_4 plant abundance.

$\delta^{13}C_{pc}$ (J.W.M., N.E.L., and E.J.B.)

Pedogenic carbonates (pc) (n = 8) were collected and analyzed for carbon isotopic composition from the Bk horizons (zones of accumulation of carbonate) of eight paleosols focused on the interval from 642 to 261 ka ago. Pedogenic carbonate was collected at least 50 cm below the top of each paleosol (or a conservative estimate of the top) to ensure that $\delta^{13}C$ values of pedogenic carbonates ($\delta^{13}C_{pc}$) reflect

the isotopic composition of vegetation and not that of atmospheric CO_2 (*85*). These carbonates, which were at various stages of development, were sampled throughout the Bk horizons of moderately well-developed paleosols, with ped development and horizonation caused by the dissolution of carbonate and reprecipitation at depth. These Bk horizons showed increased Ca content at depth in scanning XRF unrelated to the parent material. These carbonates were also identified as pedogenic in origin by their size ($\lesssim$2 cm), micritic texture, and the incorporation of soil matrix into the carbonate material as they grew over time. Pedogenic carbonates less than 50 cm below the top of the paleosol, larger than 2 cm, or with sparry textures were excluded from analysis to avoid any potential for diagenetic alteration. Samples were powdered, homogenized, and dried at 40°C for 24 hours before analysis. Powders were digested in 100‰ phosphoric acid at 70°C in single reaction vessels using a NuCarb device. Carbon and oxygen isotope ratios of the resultant CO_2 were analyzed on a Nu Perspective gas source IRMS at the University of Michigan, Ann Arbor. Although not highlighted in this paper, $\delta^{18}O$ values of these samples are also reported here for completeness. A calcite working standard was measured every sixth sample and at the beginning and end of each analytical run, yielding a standard deviation of 0.03‰ (1σ) for $\delta^{13}C$ and 0.11‰ (1σ) for $\delta^{18}O$, where $\delta = [R_{sample}/R_{standard} - 1] \times 1000$. Carbon and oxygen isotope ratios of all samples were normalized via two-point linear calibration using international standards NBS-18 ($\delta^{13}C = -5.014‰$; $\delta^{18}O = -23.2‰$) and NBS-19 ($\delta^{13}C = 1.95‰$; $\delta^{18}O = -2.20‰$). For each paleosol with pedogenic carbonate, powders from two to nine unique carbonate samples were analyzed. Pedogenic carbonate samples include distinct nodules collected at discrete depths in the core and aggregates of less indurated carbonate material collected over 3- to 25-cm intervals within a single Bk horizon, as denoted in sample IDs. Each unique sample was analyzed in duplicate, yielding a mean intersample difference in $\delta^{13}C_{pc}$ of 0.14‰ and $\delta^{18}O_{pc}$ of 0.17‰. The mean $\delta^{13}C_{pc}$ values and 1σ SDs of the analyses from these multiple nodules are plotted in Fig. 3. All $\delta^{13}C_{pc}$ and $\delta^{18}O_{pc}$ values are reported in ‰ relative to the VPDB standard. Age designations for mean pedogenic $\delta^{13}C_{pc}$ values are shown at the midpoint of paleosol age durations.

X-radiography and XRF core scanning (M.S. and E.T.B.)

The ITRAX XRF core scanner of the Large Lake Observatory, Duluth, MN, was used to measure bulk concentrations of major elements (e.g., Si, K, and Ca) on split core surfaces (n = 12,218) and to create x-radiographic images. X-radiographs were collected with 0.2-mm resolution (step size), with 60 kV, 50 mA, and exposure time ranging from 200 to 1500 ms. XRF data were collected at 1-cm resolution (step size) using the Mo x-ray tube with 30 kV, 20 mA, 60-s exposure time. Three National Institute of Standards and Technology Certified Reference Materials or Standard Reference Materials (SRM) with properties similar to the sediment cores were used to calibrate the elemental raw counts. The Si/K ratio reflects diatom productivity and preservation. High (low) Si/K may be interpreted to reflect an oligotropic, relatively fresh (eutrophic and alkaline) lake at the time of deposition. The good correlation of Si/K to diatom counts (by R.B.O. and V.M.) indicates an insignificant influence of biogenic silica from phytoliths or of quartz. The times series of %Ca (dominated by calcium carbonate content) can reflect autochthonous carbonate precipitation within a lake and/or carbonate nodules formed during postdepositional early diagenesis or pedogenesis. In sections that were not significantly affected by pedogenesis, we propose two scenarios to interpret %Ca variability: In periods when both Si/K and Ca% are high, carbonate precipitation was likely triggered by photosynthesis in a eutrophic, relatively fresh lake. By contrast, in intervals of low Si/K and high %Ca, carbonate precipitation was likely triggered by oversaturation in a relatively saline, alkaline lake.

X-ray diffraction (N.R. and D.D.)

Samples for XRD analysis were collected at 48-cm intervals and at higher resolution within sections of laminated lacustrine muds. A total of 402 samples were oven dried at 40°C for 48 hours and then ground to fine powder using ball and pestle impact grinders or mortar and pestle. At Georgia State University, the bulk mineralogy of core material was analyzed by powder XRD using a Panalytical X'pert Pro MPD using CuKα radiation, in the range 5°–70° 2θ, operating at 45 kV and 40 mA with a total scan time of 30 min. Powder diffraction patterns were analyzed using PANalytical High Score software suite with reference to PDF-2 database (*86*, *87*).

SUPPLEMENTARY MATERIALS

Supplementary material for this article is available at http://advances.sciencemag.org/cgi/content/full/6/43/eabc8975/DC1

REFERENCES AND NOTES

1. E. S. Vrba, in *Paleoclimate and Evolution, with Emphasis on Human Origins*, E. S. Vrba, G. H. Denton, T. C. Partridge, L. H. Burckle, Eds. (Yale Univ. Press, 1995), pp. 24–45.
2. P. B. deMenocal, Plio-Pleistocene African climate. *Science* **270**, 53–59 (1995).
3. P. B. deMenocal, Climate and human evolution. *Science* **331**, 540–542 (2011).
4. M. H. Trauth, M. A. Maslin, A. L. Deino, M. R. Strecker, A. G. N. Bergner, M. Dühnforth, High- and low-latitude forcing of Plio-Pleistocene East African climate and human evolution. *J. Hum. Evol.* **53**, 475–486 (2007).
5. R. Potts, J. T. Faith, Alternating high and low climate variability: The context of natural selection and speciation in Plio-Pleistocene hominin evolution. *J. Hum. Evol.* **87**, 5–20 (2015).
6. A. S. Brooks, J. E. Yellen, R. Potts, A. K. Behrensmeyer, A. L. Deino, D. E. Leslie, S. H. Ambrose, J. R. Ferguson, F. d'Errico, A. M. Zipkin, S. Whittaker, J. Post, E. G. Veatch, K. Foecke, J. B. Clark, Long-distance stone transport and pigment use in the earliest Middle Stone Age. *Science* **360**, 90–94 (2018).
7. R. Potts, A. K. Behrensmeyer, J. T. Faith, C. A. Tryon, A. S. Brooks, J. E. Yellen, A. L. Deino, R. Kinyanjui, J. B. Clark, C. M. Haradon, N. E. Levin, H. J. M. Meijer, E. G. Veatch, R. B. Owen, R. W. Renaut, Environmental dynamics during the onset of the Middle Stone Age in eastern Africa. *Science* **360**, 86–90 (2018).
8. A. L. Deino, A. K. Behrensmeyer, A. S. Brooks, J. E. Yellen, W. D. Sharp, R. Potts, Chronology of the Acheulean to Middle Stone Age transition in Eastern Africa. *Science* **360**, 95–98 (2018).
9. C. M. Schlebusch, H. Malmström, T. Günther, P. Sjödin, A. Coutinho, H. Edlund, A. R. Munters, M. Vicente, M. Steyn, H. Soodyall, M. Lombard, M. Jakobsson, Southern African ancient genomes estimate modern human divergence to 350,000 to 260,000 years ago. *Science* **358**, 652–655 (2017).
10. D. Richter, R. Grün, R. Joannes-Boyau, T. E. Steele, F. Amani, M. Rué, P. Fernandes, J.-P. Raynal, D. Geraads, A. Ben-Ncer, J.-J. Hublin, S. P. McPherron, The age of the hominin fossils from Jebel Irhoud, Morocco, and the origins of the Middle Stone Age. *Nature* **546**, 293–296 (2017).
11. R. Grün, A. Pike, F. McDermott, S. Eggins, G. Mortimer, M. Aubert, L. Kinsley, R. Joannes-Boyau, M. Rumsey, C. Denys, J. Brink, T. Clark, C. Stringer, Dating the skull from Broken Hill, Zambia, and its position in human evolution. *Nature* **580**, 372–375 (2020).
12. P. H. G. M. Dirks, E. M. Roberts, H. Hilbert-Wolf, J. D. Kramers, J. Hawks, A. Dosseto, M. Duval, M. Elliott, M. Evans, R. Grün, J. Hellstrom, A. I. R. Herries, R. Joannes-Boyau, T. V. Makhubela, C. J. Placzek, J. Robbins, C. Spandler, J. Wiersma, J. Woodhead, L. R. Berger, The age of *Homo naledi* and associated sediments in the Rising Star Cave, South Africa. *eLife* **6**, e24231 (2017).
13. S. McBrearty, A. S. Brooks, The revolution that wasn't: A new interpretation of the origin of modern human behavior. *J. Hum. Evol.* **39**, 453–563 (2000).
14. J. Blinkhorn, M. Grove, The structure of the Middle Stone Age of eastern Africa. *Quat. Sci. Rev.* **195**, 1–20 (2018).

15. P. Shipman, R. Potts, M. Pickford, Lainyamok: A new middle Pleistocene hominid site. *Nature* **306**, 365–368 (1983).
16. R. Potts, P. Shipman, E. Ingall, Taphonomy, paleoecology and hominids of Lainyamok, Kenya. *J. Hum. Evol.* **17**, 597–614 (1988).
17. C. Stringer, The origin and evolution of *Homo sapiens*. *Phil. Trans. R. Soc. B* **371**, 20150237 (2016).
18. B. H. Baker, J. G. Mitchell, L. A. J. Williams, Stratigraphy, geochronology and volcano-tectonic evolution of the Kedong-Naivasha-Kinangop region, Gregory Rift Valley, Kenya. *J. Geol. Soc.* **145**, 107–116 (1988).
19. A. L. Deino, R. Dommain, C. B. Keller, R. Potts, A. K. Behrensmeyer, E. J. Beverly, J. King, C. W. Heil, M. Stockhecke, E. T. Brown, J. Moerman, P. deMenocal; Olorgesailie Drilling Project Scientific Team, Chronostratigraphic model of a high-resolution drill core record of the past million years from the Koora Plain, south Kenya Rift: Overcoming the difficulties of variable sedimentation rate and hiatuses. *Quat. Sci. Rev.* **215**, 213–231 (2019).
20. A. Cohen, C. Campisano, R. Arrowsmith, A. Asrat, A. K. Behrensmeyer, A. Deino, C. Feibel, A. Hill, R. Johnson, J. Kingston, H. Lamb, T. Lowenstein, A. Noren, D. Olago, R. B. Owen, R. Potts, K. Reed, R. Renaut, F. Schäbitz, J.-J. Tiercelin, M. H. Trauth, J. Wynn, S. Ivory, K. Brady, R. O'Grady, J. Rodysill, J. Githiri, J. Russell, V. Foerster, R. Dommain, S. Rucina, D. Deocampo, J. Russell, A. Billingsley, C. Beck, G. Dorenbeck, L. Dullo, D. Feary, D. Garello, R. Gromig, T. Johnson, A. Junginger, M. Karanja, E. Kimburi, A. Mbuthia, T. McCartney, E. McNulty, V. Muiruri, E. Nambiro, E. W. Negash, D. Njagi, J. N. Wilson, N. Rabideaux, T. Raub, M. J. Sier, P. Smith, J. Urban, M. Warren, M. Yadeta, C. Yost, B. Zinaye, The hominin sites and Paleolakes Drilling Project: Inferring the environmental context of human evolution from eastern African rift lake deposits. *Sci. Dril.* **21**, 1–16 (2016).
21. L. R. Binford, *Constructing Frames of Reference: An Analytical Method for Archaeological Theory Building Using Ethnographic and Environmental Data Sets* (University of California Press, 2001).
22. F. W. Marlowe, Hunter-gatherers and human evolution. *Evol. Anthropol.* **14**, 54–67 (2005).
23. R. L. Kelly, *The Foraging Spectrum: Diversity in Hunter-gatherer Lifeways* (Cambridge Univ. Press, ed. 2, 2013).
24. R. Dyson-Hudson, E. A. Smith, Human territoriality: An ecological reassessment. *Am. Anthropol.* **80**, 21–41 (1978).
25. D. Western, Water availability and its influence on the structure and dynamics of a savannah large mammal community. *Afr. J. Ecol.* **13**, 265–286 (1975).
26. S. C. Fritz, S. Juggins, R. W. Battarbee, D. R. Engstrom, Reconstruction of past changes in salinity and climate using a diatom-based transfer function. *Nature* **352**, 706–708 (1991).
27. E. A. Kellogg, C_4 photosynthesis. *Curr. Biol.* **23**, R594–R599 (2013).
28. D. Barboni, R. Bonnefille, A. Alexandre, J. D. Meunier, Phytoliths as paleoenvironmental indicators, West Side Middle Awash Valley, Ethiopia. *Palaeogeogr. Palaeoclimatol. Palaeoecol.* **152**, 87–100 (1999).
29. L. Bremond, A. Alexandre, O. Peyron, J. Guiot, Grass water stress estimated from phytoliths in West Africa. *J. Biogeogr.* **32**, 311–327 (2005).
30. L. Bremond, A. Alexandre, C. Hély, J. Guiot, A phytolith index as a proxy of tree cover density in tropical areas: Calibration with Leaf Area Index along a forest-savanna transect in southeastern Cameroon. *Glob. Planet. Change* **45**, 277–293 (2005).
31. A. Alexandre, J.-D. Meunier, A.-M. Lézine, A. Vincens, D. Schwartz, Phytoliths: Indicators of grassland dynamics during the late Holocene in intertropical Africa. *Palaeogeogr. Palaeoclimatol. Palaeoecol.* **136**, 213–219 (1997).
32. P. C. Tzedakis, V. Margari, D. A. Hodell, Coupled ocean–land millennial-scale changes 1.26 million years ago, recorded at Site U1385 off Portugal. *Glob. Planet. Change* **135**, 83–88 (2015).
33. M. Hyodo, B. Bradák, M. Okada, S. Katoh, I. Kitaba, D. L. Dettman, H. Hayashi, K. Kumazawa, K. Hirose, O. Kazaoka, K. Shikoku, A. Kitamura, Millennial-scale northern Hemisphere Atlantic-Pacific climate teleconnections in the earliest Middle Pleistocene. *Sci. Rep.* **7**, 10036 (2017).
34. A. K. Behrensmeyer, R. Potts, A. Deino, The Oltulelei Formation of the southern Kenyan Rift Valley: A chronicle of rapid landscape transformation over the last 500 k.y. *Geol. Soc. Am. Bull.* **130**, 1474–1492 (2018).
35. B. H. Baker, in *Sedimentation in the African Rifts*, L. E. Frostick, R. W. Renaut, I. Reid, J. J. Tiercelin, Eds. (Blackwell Scientific Publications, 1986), pp. 45–57.
36. L. A. Olaka, E. O. Odada, M. H. Trauth, D. O. Olago, The sensitivity of East African rift lakes to climate fluctuations. *J. Paleolimnol.* **44**, 629–644 (2010).
37. R. B. Owen, V. M. Muiruri, T. K. Lowenstein, R. W. Renaut, N. Rabideaux, S. Luo, A. L. Deino, M. J. Sier, G. Dupont-Nivet, E. P. McNulty, K. Leet, A. Cohen, C. Campisano, D. Deocampo, C.-C. Shen, A. Billingsley, A. Mbuthia, Progressive aridification in East Africa over the last half million years and implications for human evolution. *Proc. Natl. Acad. Sci. U.S.A.* **115**, 11174–11179 (2018).
38. S. J. McNaughton, Ecology of a grazing ecosystem: The Serengeti. *Ecol. Monogr.* **55**, 259–294 (1985).
39. C. Coetsee, W. D. Stock, J. M. Craine, Do grazers alter nitrogen dynamics on grazing lawns in a South African savannah? *Afr. J. Ecol.* **49**, 62–69 (2011).
40. G. P. Hempson, S. Archibald, W. J. Bond, R. P. Ellis, C. C. Grant, F. J. Kruger, L. M. Kruger, C. Moxley, N. Owen-Smith, M. J. S. Peel, I. P. J. Smit, K. J. Vickers, Ecology of grazing lawns in Africa. *Biol. Rev.* **90**, 979–994 (2015).
41. L. Werdelin, W. J. Sanders, *Cenozoic Mammals of Africa* (University of California Press, 2010).
42. R. Potts, Variability selection in hominid evolution. *Evol. Anthropol.* **7**, 81–96 (1998).
43. R. Potts, A. Deino, Mid-Pleistocene change in large mammal faunas of East Africa. *Quatern. Res.* **43**, 106–113 (1995).
44. J. D. Clark, Y. Beyene, G. WoldeGabriel, W. K. Hart, P. R. Renne, H. Gilbert, A. Defleur, G. Suwa, S. Katoh, K. R. Ludwig, J.-R. Boisserie, B. Asfaw, T. D. White, Stratigraphic, chronological and behavioural contexts of Pleistocene *Homo sapiens* from Middle Awash, Ethiopia. *Nature* **423**, 747–752 (2003).
45. C. A. Tryon, J. T. Faith, Variability in the Middle Stone Age of eastern Africa. *Curr. Anthropol.* **54**, S234–S254 (2013).
46. MathWorks, MATLAB Release 2018a (The MathWorks, Inc., 2018).
47. F. Gasse, *Les diatomées lacustres Plio-Pléistocènes du Gadeb (Ethiopie): Systématique, paléoécologie, biostratigraphie* (Revue Algologique, 1980).
48. F. Gasse, *East African Diatoms: Taxonomy, Ecological Distribution* (J. Cramer, Stuttgart, 1986), Bibliotheca Diatomologica, vol. 11.
49. O. Katz, D. Cabanes, S. Weiner, A. M. Maeir, E. Boaretto, R. Shahack-Gross, Rapid phytolith extraction for analysis of phytolith concentrations and assemblages during an excavation: An application at Tell es-Safi/Gath, Israel. *J. Archaeol. Sci.* **37**, 1557–1563 (2010).
50. R. N. Kinyanjui, thesis, University of Witwatersrand (2018); https://t.co/JxhDDR5olF.
51. M. Madella, A. Alexandre, T. Ball, International code for phytolith nomenclature 1.0. *Ann. Bot.* **96**, 253–260 (2005).
52. P. C. Twiss, E. Suess, R. M. Smith, Morphological classification of grass phytoliths. *Soil Sci. Soc. Am. J.* **33**, 109–115 (1969).
53. P. C. Twiss, in *Phytolith Systematics: Emerging Issues*, G. Rapp Jr., S. C. Mulholland, Eds. (Plenum Press, 1992), pp. 113–128.
54. L. Rossouw, thesis, University of the Free State (2009); https://scholar.ufs.ac.za/xmlui/handle/11660/4013.
55. G. Rapp Jr., S. C. Mulholland, *Phytolith Systematics: Emerging Issues* (Plenum Press, 1992).
56. G. G. Fredlund, L. T. Tieszen, Modern phytolith assemblages from the North American Great Plains. *J. Biogeogr.* **21**, 321–335 (1994).
57. G. G. Fredlund, L. T. Tieszen, Calibrating grass phytolith assemblages in climatic terms: Application to Late Pleistocene assemblage from Kansas and Nebraska. *Palaeogeogr. Palaeoclimatol. Palaeoecol.* **136**, 199–211 (1997).
58. D. Barboni, L. Bremond, R. Bonnefille, Comparative study of modern phytolith assemblages from inter-tropical Africa. *Palaeogeogr. Palaeoclimatol. Palaeoecol.* **246**, 454–470 (2007).
59. F. Runge, The opal phytolith inventory of soils in central Africa—Quantities, shapes, classification, and spectra. *Rev. Palaeobot. Palynol.* **107**, 23–53 (1999).
60. D. R. Piperno, *Phytoliths: A Comprehensive Guide for Archaeologists and Paleoecologists* (AltaMira Press, 2006).
61. R. M. Albert, M. K. Bamford, D. Cabanes, Taphonomy of phytoliths and macroplants in different soils from Olduvai Gorge (Tanzania) and the application to Plio-Pleistocene palaeoanthropological samples. *Quat. Int.* **148**, 78–94 (2006).
62. D. Barboni, L. Bremond, Phytoliths of East African grasses: An assessment of their environmental and taxonomic significance based on floristic data. *Rev. Palaeobot. Palynol.* **158**, 29–41 (2009).
63. C. A. E. Strömberg, thesis, University of California Berkeley (2003).
64. K. Neumann, A. Fahmy, L. Lespez, A. Ballouche, E. Huysecom, The Early Holocene palaeoenvironment of Ounjougou (Mali): Phytoliths in a multiproxy context. *Palaeogeogr. Palaeoclimatol. Palaeoecol.* **276**, 87–106 (2009).
65. J. Mercader, T. Bennett, C. Esselmont, S. Simpson, D. Walde, Phytoliths in woody plants from the Miombo woodlands of Mozambique. *Ann. Bot.* **104**, 91–113 (2009).
66. J. Mercader, F. Astudillo, M. Barkworth, T. Bennett, C. Esselmont, R. Kinyanjui, D. Laskin Grossman, S. Simpson, D. Walde, Poaceae phytoliths from the Niassa Rift, Mozambique. *J. Archaeol. Sci.* **37**, 1953–1967 (2010).
67. G. M. Ashley, D. Barboni, M. Dominguez-Rodrigo, H. T. Bunn, A. Z. P. Mabulla, F. Diez-Martin, R. Barba, E. Baquedano, Spring and wooded habitats at FLK Zinj and their relevance to origins of human behavior. *Quatern. Res.* **74**, 304–314 (2010).
68. G. M. Ashley, D. Barboni, M. Dominguez-Rodrigo, H. T. Bunn, A. Z. P. Mabulla, F. Diez-Martin, R. Barba, E. Baquedano, Paleoenvironmental and paleoecological reconstruction of a freshwater oasis in savannah grassland at FLK North, Olduvai Gorge, Tanzania. *Quatern. Res.* **74**, 333–343 (2010).
69. R. N. Kinyanjui, thesis, University of Cape Town (2012); http://www.pcu.uct.ac.za/sites/default/files/image_tool/images/192/Kinyanjui%202011.pdf.

70. A. Novello, D. Barboni, L. Berti-Equille, J.-C. Mazur, P. Poilecot, P. Vignaud, Phytolith signal of aquatic plants and soils in Chad, Central Africa. *Rev. Palaeobot. Palynol.* **178**, 43–58 (2012).
71. E. C. Grimm, *Tilia and Tiliagraph* (Illinois State Museum, Springfield, 1991), vol. 101.
72. K. Faegri, J. Iverson, *Textbook of Pollen Analysis* (Blackwell Scientific Publications, 1975).
73. Soil Survey Staff, *Illustrated Guide to Soil Taxonomy, version 1* (USDA, NRCS, National Soil Survey Center, 2014).
74. D. M. Cleveland, S. C. Atchley, L. C. Nordt, Continental sequence stratigraphy of the Upper Triassic (Norian–Rhaetian) Chinle strata, Northern New Mexico, U.S.A.: Allocyclic and autocyclic origins of paleosol-bearing alluvial successions. *J. Sediment. Res.* **77**, 909–924 (2007).
75. R. L. Lupien, J. M. Russell, C. Feibel, C. Beck, I. Castañeda, A. Deino, A. S. Cohen, A leaf wax biomarker record of early Pleistocene hydroclimate from West Turkana, Kenya. *Quat. Sci. Rev.* **186**, 225–235 (2018).
76. M. M. Bender, Variations in the $^{13}C/^{12}C$ ratios of plants in relation to the pathway of photosynthetic carbon dioxide fixation. *Phytochemistry* **10**, 1239–1244 (1971).
77. J. W. Collister, G. Rieley, B. Stern, G. Eglinton, B. Fry, Compound-specific $\delta^{13}C$ analyses of leaf lipids from plants with differing carbon dioxide metabolisms. *Org. Geochem.* **21**, 619–627 (1994).
78. K. T. Uno, P. J. Polissar, E. Kahle, C. Feibel, S. Harmand, H. Roche, P. B. deMenocal, A Pleistocene palaeovegetation record from plant wax biomarkers from the Nachukui Formation, West Turkana, Kenya. *Phil. Trans. R. Soc. B* **371**, 20150235 (2016).
79. Y. Chikaraishi, H. Naraoka, S. R. Poulson, Hydrogen and carbon isotopic fractionations of lipid biosynthesis among terrestrial (C_3, C_4, and CAM) and aquatic plants. *Phytochemistry* **65**, 1369–1381 (2004).
80. J. M. Russell, H. Vogel, B. L. Konecky, S. Bijaksana, Y. Huang, M. Melles, N. Wattrus, K. Costa, J. W. King, Glacial forcing of central Indonesian hydroclimate since 60,000 y B.P. *Proc. Natl. Acad. Sci. U.S.A.* **111**, 5100–5105 (2014).
81. A. Vogts, H. Moossen, F. Rommerskirchen, J. Rullkötter, Distribution patterns and stable carbon isotopic compositions of alkanes and alkane-1-oils from plant waxes of African rain forest and savannah C_3 species. *Org. Geochem.* **40**, 1037–1054 (2009).
82. P. A. Meyers, J. L. Teranes, in *Tracking Environmental Change Using Lake Sediments: Volume 2: Physical and Geochemical Methods*, W. M. Last, J. P. Smol, Eds. (Kluwer, 2001), pp. 239–270.
83. J. M. Russell, S. J. McCoy, D. Verschuren, I. Bessems, Y. Huang, Human impacts, climate change, and aquatic ecosystem response during the past 2000 yr at Lake Wandakara, Uganda. *Quatern. Res.* **72**, 315–324 (2009).
84. M. Webb, P. A. Barker, P. M. Wynn, O. Heiri, M. van Hardenbroek, F. Pick, J. M. Russell, A. W. Stott, M. J. Leng, Interpretation and application of carbon isotope ratios in freshwater diatom silica. *J. Quat. Sci.* **31**, 300–309 (2016).
85. T. E. Cerling, Carbon dioxide in the atmosphere: Evidence from Cenozoic and Mesozoic paleosols. *Am. J. Sci.* **291**, 377–400 (1991).
86. D. M. Moore, R. C. Reynolds Jr., *X-ray Diffraction and the Identification and Analysis of Clay Minerals* (Oxford Univ. Press, ed. 2, 1997).
87. G. W. Brindley, G. Brown, *Crystal Structures of Clay Minerals and their X-ray Identification* (Mineralogical Society of Great Britain and Ireland, 1980), vol. 5.
88. E. T. Brown, in *Micro-XRF Studies of Sediment Cores: Applications of a Non-destructive Tool for the Environmental Sciences*, *Developments in Paleoenvironmental Research*, I. W. Croudace, R. G. Rothwell, Eds. (Springer Netherlands, 2015), pp. 267–277.
89. T. E. Cerling, J. G. Wynn, S. A. Andanje, M. I. Bird, D. K. Korir, N. E. Levin, W. Mace, A. N. Macharia, J. Quade, C. H. Remien, Woody cover and hominin environments in the past 6 million years. *Nature* **476**, 51–56 (2011).
90. G. P. Hempson, S. Archibald, W. J. Bond, A continent-wide assessment of the form and intensity of large mammal herbivory in Africa. *Science* **350**, 1056–1061 (2015).
91. G. Child, R. Parris, E. Le Riché, Use of mineralised water by Kalahari wildlife and its effects on habitats. *Afr. J. Ecol.* **9**, 125–142 (1971).
92. W. F. de Boer, M. J. P. Vis, H. J. de Knegt, C. Rowles, E. M. Kohi, F. van Langevelde, M. Peel, Y. Pretorius, A. K. Skidmore, R. Slotow, S. E. van Wieren, H. H. T. Prins, Spatial distribution of lion kills determined by the water dependency of prey species. *J. Mammal.* **91**, 1280–1286 (2010).
93. R. Estes, *The Behavior Guide to African Mammals: Including Hoofed Mammals, Carnivores, Primates* (University of California Press, 1991).
94. J. Kingdon, *The Kingdon Field Guide to African Mammals* (Academic Press, 1997).
95. J. G. Ogg, in *The Geologic Time Scale 2012*, F. M. Gradstein, J. G. Ogg, M. D. Schmitz, G. M. Ogg, Eds. (Elsevier, 2012), pp. 85–113.
96. J. L. Kirschvink, The least-squares line and plane and the analysis of palaeomagnetic data. *Geophys. J. Int.* **62**, 699–718 (1980).
97. L. Sagnotti, Demagnetization Analysis in Excel (DAIE). *Ann. Geophys.* **56**, D0114 (2013).
98. J. D. A. Zijderveld, in *Methods in Paleomagnetism*, D. W. Collinson, K. M. Creer, S. K. Runcorn, Eds. (Elsevier, 1967), pp. 254–286.
99. L. Tauxe, C. Badgley, Stratigraphy and remanence acquisition of a palaeomagnetic reversal in alluvial Siwalik rocks of Pakistan. *Sedimentology* **35**, 697–715 (1988).
100. World Health Organization, *A Global Overview of National Regulations and Standards for Drinking-water Quality* (World Health Organization, 2018).
101. P. Duringer, M. Schuster, J. F. Genise, H. T. Mackaye, P. Vignaud, M. Brunet, New termite trace fossils: Galleries, nests and fungus combs from the Chad basin of Africa (Upper Miocene–Lower Pliocene). *Palaeogeogr. Palaeoclimatol. Palaeoecol.* **251**, 323–353 (2007).
102. J. F. Genise, *Ichnoentomology: Insect Traces in Soils and Paleosols* (Springer, 2017), Topics in Geobiology, vol. 37.
103. E. M. Roberts, C. N. Todd, D. K. Aanen, T. Nobre, H. L. Hilbert-Wolf, P. M. O'Connor, L. Tapanila, C. Mtelela, N. J. Stevens, Oligocene termite nests with *in situ* fungus gardens from the Rukwa Rift Basin, Tanzania, support a Paleogene African origin for insect agriculture. *PLOS ONE* **11**, e0156847 (2016).
104. W. A. Sands, in *Laetoli: A Pliocene Site in Northern Tanzania*, M. D. Leakey, J. M. Harris, Eds. (1987), pp. 409–433.
105. J. J. Scott, R. W. Renaut, L. A. Buatois, R. B. Owen, Biogenic structures in exhumed surfaces around saline lakes: An example from Lake Bogoria, Kenya Rift Valley. *Palaeogeogr. Palaeoclimatol. Palaeoecol.* **272**, 176–198 (2009).
106. W. R. Tschinkel, The foraging tunnel system of the Namibian Desert termite, *Baucaliotermes hainesi*. *J. Insect Sci.* **10**, 65 (2010).
107. S. C. Fritz, B. F. Cumming, F. Gasse, K. R. Laird, in *The Diatoms: Applications for the Environmental and Earth Sciences*, J. P. Smol, E. F. Stoermer, Eds. (Cambridge Univ. Press, ed. 2, 2010), pp. 186–208.
108. E. T. Brown, in *Micro-XRF Studies of Sediment Cores: Applications of a Non-destructive Tool for the Environmental Sciences*, I. W. Croudace, R. G. Rothwell, Eds. (Springer, 2015), pp. 267–277.
109. J. Laskar, P. Robutel, F. Joutel, M. Gastineau, A. C. M. Correia, B. Levrard, A long-term numerical solution for the insolation quantities of the Earth. *Astron. Astrophys.* **428**, 261–285 (2004).

Acknowledgments: The Olorgesailie Drilling Project gratefully acknowledges the National Museums of Kenya, the Oldonyo Nyokie Group Ranch, and the Olorgesailie field team led by J.M. Nume and J.N. Mativo. Research and drilling permits were provided by the Kenyan National Council for Science and Technology, the Kenya Ministry of Petroleum and Mining, and the National Environmental Management Authority of Kenya and facilitated by the National Museums of Kenya. We thank DOSECC Exploration Services for drilling supervision, Drilling and Prospecting International (DPI) for drilling services, and the LacCore and CSDCO facilities (University of Minnesota) for core handling, processing, and storage. Elevation data in Fig. 1 are based on the TanDEM-X Science DEM (DLR 2017) granted to S.R. by the German Space Agency. We are grateful for discussions with colleagues of the Hominin Sites and Paleolakes Drilling Project (HSPDP) and for comments by C. Stringer and anonymous reviewers. **Funding:** Peter Buck Fund for Human Origins Research (Smithsonian), William H. Donner Foundation (R.P.), the Ruth and Vernon Taylor Foundation (R.P.), Whitney and Betty MacMillan (R.P.), National Science Foundation grants EAR 1322017 (A.L.D.) and EAR 1349599 (D.D.), Swiss National Science Foundation grant P300P2 158501 (M.S.), Hong Kong Research Grants Council (R.B.O. and V.M.), and the Smithsonian Human Origins Program (R.P.). Funding support for A.N. and K.B.S. provided by NSF awards EAR-1338322 and EAR-1462297. **Author contributions:** R.P. and R.D. wrote the manuscript, with support from J.W.M., S.R., and A.K.B., and all authors provided edits and discussion. D.D., R.K., J.W.M., R.B.O., J.M.R., N.R., and M.S. contributed data for Fig. 3, and all authors contributed to methods, analyses, and discussion of data interpretations. R.D., S.R., Y.G., J.W.M., J.B.C., A.K.B., P.d.M., J.T.F., and R.P. developed the figures. R.P. directed and conceived the study. R.P. and A.K.B. selected the drilling location. K.B.S., R.D., A.N., and J.B.C. provided field and laboratory support. **Competing interests:** The authors declare that they have no competing interests. **Data and materials availability:** The datasets generated and analyzed during the current study are available from the corresponding author on reasonable request. Source data for Fig. 3 are provided in tables S3 through S12.

Submitted 19 May 2020
Accepted 3 September 2020
Published 21 October 2020
10.1126/sciadv.abc8975

Citation: R. Potts, R. Dommain, J. W. Moerman, A. K. Behrensmeyer, A. L. Deino, S. Riedl, E. J. Beverly, E. T. Brown, D. Deocampo, R. Kinyanjui, R. Lupien, R. B. Owen, N. Rabideaux, J. M. Russell, M. Stockhecke, P. deMenocal, J. T. Faith, Y. Garcin, A. Noren, J. J. Scott, D. Western, J. Bright, J. B. Clark, A. S. Cohen, C. B. Keller, J. King, N. E. Levin, K. Brady Shannon, V. Muiruri, R. W. Renaut, S. M. Rucina, K. Uno, Increased ecological resource variability during a critical transition in hominin evolution. *Sci. Adv.* **6**, eabc8975 (2020).

ScienceAdvances

Increased ecological resource variability during a critical transition in hominin evolution

Richard Potts, René Dommain, Jessica W. Moerman, Anna K. Behrensmeyer, Alan L. Deino, Simon Riedl, Emily J. Beverly, Erik T. Brown, Daniel Deocampo, Rahab Kinyanjui, Rachel Lupien, R. Bernhart Owen, Nathan Rabideaux, James M. Russell, Mona Stockhecke, Peter deMenocal, J. Tyler Faith, Yannick Garcin, Anders Noren, Jennifer J. Scott, David Western, Jordon Bright, Jennifer B. Clark, Andrew S. Cohen, C. Brehnin Keller, John King, Naomi E. Levin, Kristina Brady Shannon, Veronica Muiruri, Robin W. Renaut, Stephen M. Rucina and Kevin Uno

Sci Adv **6** (43), eabc8975.
DOI: 10.1126/sciadv.abc8975